



## Heat shock protein 60 couples an oxidative stress-responsive p38/MK2 signaling and NF- $\kappa$ B survival machinery in cancer cells

Seongchun Min<sup>a</sup>, Ji Yeon Kim<sup>a</sup>, Hyo Min Cho<sup>b</sup>, Sujin Park<sup>a</sup>, Ji Min Hwang<sup>a</sup>, Hyejin You<sup>c</sup>, Young Chan Chae<sup>d</sup>, Won-Jae Lee<sup>c</sup>, Woong Sun<sup>b</sup>, Dongmin Kang<sup>a</sup>, Sanghyuk Lee<sup>a</sup>, Sang Won Kang<sup>a,\*</sup>

<sup>a</sup> Department of Life Science, Ewha Womans University, Seoul, 03760, Republic of Korea

<sup>b</sup> Department of Anatomy, Korea University School of Medicine, Seoul, 02841, Republic of Korea

<sup>c</sup> National Creative Research Center for Halogenomics, School of Biological Science, Seoul National University, Seoul, 08826, Republic of Korea

<sup>d</sup> Department of Biological Sciences, UNIST, Ulsan, 44919, Republic of Korea

### ARTICLE INFO

#### Keywords:

Oxidative stress  
Mitochondria  
p38 MAPK  
HSP60  
NF- $\kappa$ B

### ABSTRACT

Mitochondria communicate with other cellular compartments via the secretion of protein factors. Here, we report an unexpected messenger role for heat shock protein 60 (HSP60) as a mitochondrial-releasing protein factor that couples stress-sensing signaling and cell survival machineries. We show that mild oxidative stress predominantly activates the p38/MK2 complex, which phosphorylates mitochondrial fission factor 1 (MFF1) at the S155 site. Such phosphorylated MFF1 leads to the oligomerization of voltage anion-selective channel 1, thereby triggering the formation of a mitochondrial membrane pore through which the matrix protein HSP60 passes. The liberated HSP60 associates with and activates the I $\kappa$ B kinase (IKK) complex in the cytosol, which consequently induces the NF- $\kappa$ B-dependent expression of survival genes in nucleus. Indeed, inhibition of the HSP60 release or HSP60-IKK interaction sensitizes the cancer cells to mild oxidative stress and regresses the tumorigenic growth of cancer cells in the mouse xenograft model. Thus, this study reveals a novel mitonuclear survival axis responding to oxidative stress.

### 1. Introduction

Aerobic organisms are constantly challenged by the presence of oxidative stress (OS), which is among key factors determining cell fate [1]. Mitochondria are the major subcellular organelles susceptible to OS [2,3]. Upon severe OS condition, the retrograde signaling by mitochondria executes programmed cell death by releasing pro-apoptotic factors, such as cytochrome *c*, apoptosis-inducing factor, and second mitochondria-derived activator of caspase (Smac)/direct inhibitor of apoptosis binding protein with low pI (DIABLO) [3]. Concomitantly, the unpaired electrons that leads to the intracellular burst of reactive oxygen species could be released by mitochondrial electron transport chain. Thus, the mitochondrial response to severe and persistent OS has been shown to be associated with various pathological conditions such as cancer and degenerative diseases [4,5]. In contrast, numerous compelling studies indicate that mild and transient OS plays a signaling role in certain physiological contexts [6]. For instance, mouse myogenic

progenitor cells selected by low H<sub>2</sub>O<sub>2</sub> treatment were shown to exhibit resistance to severe OS [7]. Some *in vivo* evidence suggests that ischemic preconditioning allows myocardial tolerance to subsequent ischemia-reperfusion injury [8,9]. However, the mechanism by which mild OS modulates the cell survival is largely unknown.

Heat shock protein 60 (HSP60) is a nuclear-encoded mitochondrial protein that functions as a molecular chaperone in the matrix compartment [10]. Nonetheless, a number of studies reported the extra-mitochondrial presence of HSP60 in various cell types [11–13]. Unintentionally, we have identified the HSP60 protein as a component in the cytosolic I $\kappa$ B kinase (IKK) complex through a proteomics screening [14]. Given that IKK/nuclear factor- $\kappa$ B (NF- $\kappa$ B) axis is the major cell survival pathway [15,16], we hypothesized that HSP60 could have a role as a candidate for mitochondrial-derived survival factor, which has thus far remained identified.

In this study, we found that in the mild OS-challenged cancer cells mitochondria liberated HSP60 to cytosol. The HSP60 release occurred through the assembly of a voltage anion-selective channel 1 (VDAC1)-

\* Corresponding author.

E-mail address: [kangsw@ewha.ac.kr](mailto:kangsw@ewha.ac.kr) (S.W. Kang).

<https://doi.org/10.1016/j.redox.2022.102293>

Received 27 January 2022; Received in revised form 10 March 2022; Accepted 15 March 2022

Available online 18 March 2022

2213-2317/© 2022 The Authors. Published by Elsevier B.V. This is an open access article under the CC BY-NC-ND license (<http://creativecommons.org/licenses/by-nc-nd/4.0/>).

### Abbreviations

ANT	Adenine nucleotide translocase
EGFP	Enhanced green fluorescence protein
MBP	Myelin basic protein
MTS	Mitochondrial targeting signal
OS	Oxidative stress
PH	Pleckstrin homology
PLA	Proximity ligation assay
VDAC	Voltage-dependent anion channel

centered membrane pore driven by the p38/MK2-dependent phosphorylation of mitochondrial fission factor 1 (MFF1). Consequently, the released HSP60 associated with and activated the IKK complex, which resulted in the induction of the NF- $\kappa$ B-dependent gene expression.

## 2. Materials and methods

### 2.1. Reagents and antibodies

Antibodies against VDAC1 (B-6), IKK $\alpha$ / $\beta$  (H-470), IKK $\beta$  (H-4), IKK $\gamma$  (FL-419, B-3), HSP60 (K-19 and N-20), I $\kappa$ B $\alpha$  (C-21), Bcl-2, Bcl-xL, Cyclophilin D, c-Src, Enhanced green fluorescence protein (EGFP), MK2, p-MK2, and goat IgG were purchased from Santa Cruz Biotechnology (Dallas, TX, USA). Antibodies against p-IKK $\alpha$ / $\beta$ , p-I $\kappa$ B $\alpha$ , ANT2 (E2B9D), Bax, p-Src (Y416), p-JNK (T183/Y185), JNK1/2, p38, and p-p38 were from Cell Signaling Technology (Danvers, MA, USA). Anti-cytochrome c antibody was from BD Bioscience (San Jose, CA, USA). Antibodies to Prx III and  $\beta$ -actin were obtained from AbFrontier (Seoul, Korea). Anti-MFF1 antibody was purchased from Proteintech (Rosemont, IL, USA). Recombinant GST-fused p38 enzyme was purchased from R&D systems (Minneapolis, MN, USA).

Mouse monoclonal antibody against  $\alpha$ -tubulin, hydrogen peroxide, glucose oxidase, diamide, cyclosporine A, cycloheximide, coomassie brilliant blue R250, and DuoLink *in situ* fluorescence reagent were purchased from Sigma-Aldrich (St. Louis, MO, USA). SB203580, MG132, bongkrekic acid, lactacystin, bafilomycin A1, and 4,4'-diisothiocyanostilbene-2,2'-disulfonic acid were purchased from Calbiochem (San Diego, CA, USA). Tetramethylrhodamine, ethyl ester (TMRE) was purchased from Invitrogen (Waltham, MA, USA). MK inhibitor IV was purchased from Cayman Chemical (Ann Arbor, MI, USA).

### 2.2. Plasmid construction

The full-length cDNA of human HSP60 was obtained from the National Genome Information Center (Daejeon, Korea). The plasmid harboring hemagglutinin (HA)-tagged HSP60 sequence was produced by following procedures: pcDNA3-MTS-HA was generated by insertion of mitochondrial targeting signal (MTS) sequence (amino acid 1–26 based on human HSP60 sequence) into pcDNA3-HA vector (Invitrogen, USA) using *HindIII* and *KpnI* enzymes. The residual open reading sequence of human HSP60 (amino acid 27–573, designated as HSP60c) was then subcloned into pcDNA3-MTS-HA vector using *EcoRV* and *XhoI* enzymes, resulting the expression vector pcDNA3-MTS-HA-HSP60<sup>WT</sup>. In addition, the pcDNA3 vector encoding MTS-HA-HSP60<sup>D423A</sup> was generated by site-directed mutagenesis (QuikChange mutagenesis kit, Stratagene). For live-cell imaging, the EGFP and PLC $\delta$ 1-PH domains were tandemly subcloned between MTS and HSP60 using *EcoRI/KpnI* and *KpnI/EcoRV* enzyme pair, respectively. The DsRed-PH plasmid for pre-labeling the plasma membrane was generated by insertion of PLC $\delta$ 1-PH domain into DsRed-N1 vector (Clontech).

The retroviral vectors encoding the truncated HSP60 mutant lacking MTS (HSP60c) and release-blocking mutant (D423A) of HSP60 were

constructed by subcloning the corresponding regions (*italicized*) from pcDNA3-MTS-HA-HSP60 and pcDNA3-MTS-HA-HSP60<sup>D423A</sup>, respectively, into the pQCXIP plasmid (Clontech). The retroviral vectors were transfected into the 293T cells along with retrovirus packing plasmids (VSVG and gag/pol) according to the manufacturer's protocol. The culture supernatants containing the retrovirus particles were collected and frozen until use.

The full length of human VDAC1 vector was kindly provided by Prof. Jong Kyung Chung (Seoul National University, Korea). Flag-tagged VDAC1 was constructed by PCR and subcloning into pFLAG-CMV2 vector using *NotI* and *BamHI* enzymes.

Human MFF1 open reading frame sequence (NM\_001277061) cloned in the mammalian expression vector pEZ-M12 (Genecopoeia, USA) was subjected to the site-directed mutagenesis using the following primer sets: (forward) 5'-gatcttgaccttattcaggcagctcccttaaacccctggca-3' and (reverse) 5'-tgccaggggttaaaggagctgctgaataaggtcaagatc-3' for MFF1-S105A/T106A, (forward) 5'-gatttagaaagacctctgcagccctcaaaatgaa-gaatc-3' and (reverse) 5'-gatttctctattttaggggctgcaggaggtcttctaatac-3' for MFF1-T137A/T138A, (forward) 5'-ccctggcactgaaagcaccacctgtg-tacttac-3' and (reverse) 5'-gtaagtagcacaggtggtcttctcagtcagggg-3' for MFF1-T115A. Full-length human MFF1 sequence was subcloned into the pGEX4T-1 vector for bacterial expression by PCR cloning using the following primers: (Forward) 5'-tcgcgatccatgagtaaaggaacaagcag-3' and (Reverse) 5'-tatagcggccgcttagcggcgaaaccagagcc-3' for wild type (WT), 5'-tatagcggccgcttaggcagaatctgatctgtgcc-3' for MFF1-180, 5'-tatagcggccgcttaaactctcttggaaactcttg-3' for MFF1-100, and 5'-tatagcggccgcttaaactctcttggaaactcttg-3' for MFF1-70, where *BamHI* and *NotI* are underlined.

For all constructs, the correct sequences of constructs were validated by DNA sequencing (Macrogen, Seoul, Korea). The puro plasmids encoding human Bcl-2 or Bcl-XL were kindly provided by Prof. Duck Young Shin (Dankook University, Korea). The pGEX4T plasmid encoding GST-I $\kappa$ B $\alpha$  (1–54) were previously described [14].

### 2.3. Cell culture

HeLa, HCT116, HepG2, MDA-MB-231, PC3, and LNCaP cells were obtained from the American Type Culture Collection (Rockville, MD, USA). Except HCT116 cells maintained in McCoy 5a medium, other cells were maintained in DMEM supplemented with 10% (v/v) fetal bovine serum, 100 units/mL penicillin, and 100  $\mu$ g/mL streptomycin in a humidified atmosphere containing 5% CO<sub>2</sub>. Bax<sup>+/+</sup> and Bax<sup>-/-</sup> HCT116 cells were kindly provided by Bert Vogelstein (Johns Hopkins University, USA). Mycoplasma contamination was periodically tested in the cell culture supernatants using mycoplasma detection kit (Biotool, USA).

HeLa-Luc stable cell lines expressing release-blocking mutant (D423A) of human HSP60 were produced by infection of retroviruses encoding MTS-HA-HSP60<sup>D423A</sup> sequence.

### 2.4. Cell viability assay

Cells were stimulated with H<sub>2</sub>O<sub>2</sub> at indicated concentrations for 24 h and collected by pipetting following incubation with 0.05% trypsin-EDTA solution for 2 min. The collected cells were harvested in the 5-ml FACS tubes by centrifugation. The cell pellets were re-suspended in cold PBS and then stained using annexin V-FITC apoptosis detection kit I (BD Pharmingen) according to manufacturer's protocol. The stained cells were analyzed using a FACSCalibur system (Becton Dickinson). The percent of viable cells was determined by the equation of [100 - percent of PI/annexin-V-positive cells].

### 2.5. Antibody transduction

The cellular transduction of control IgG or HSP60-specific antibody ( $\alpha$ -HSP60 N) was achieved using a Chariot<sup>TM</sup> protein delivery kit (Active Motif). In brief, 2  $\times$  10<sup>5</sup> of cells per well were seeded into 6-well plate.

After 24 h, cells were incubated with 200  $\mu$ l of antibody/Chariot complexes (1:2 w/w) in serum free medium for 3 h at 37 °C. Negative control samples were treated with normal goat IgG instead of the anti-HSP60 antibody.

## 2.6. Subcellular fractionation

The cytosolic and mitochondrial fractions were separated using ProteoExtract subcellular proteome extraction kit (Calbiochem). Briefly, cells were harvested and washed twice with a wash buffer. After washing, the cells were re-suspended in 50  $\mu$ l of Extraction Buffer I containing protease inhibitor cocktail and lysed by gently rocking for 5 min. Cell debris and heavy membrane organelles were pelleted from the first lysates by centrifugation at 1000 $\times$ g for 10 min. The supernatant containing cytosolic fraction was transferred to a new tube. Then, the pellet was re-suspended in 50  $\mu$ l of Extraction Buffer II containing protease inhibitor cocktail and lysed by gently rocking for 10 min. The second pellet containing mitochondrial fraction was obtained by centrifugation at 6000 $\times$ g for 10 min. The purity of cytosolic and mitochondrial fractions was verified by specific markers:  $\alpha$ -tubulin for cytosol, peroxiredoxin III (Prx III) for mitochondrial matrix, and VDAC1 for mitochondrial outer membrane. To achieve an optimum comparison in immunoblotting, the mitochondrial fractions were diluted by five-fold.

## 2.7. Immunoblot and immunoprecipitation

Cells were rinsed once with ice-cold phosphate-buffered saline (PBS) and then lysed in a lysis buffer containing 20 mM Hepes (pH 7.0), 1% Triton X-100, 150 mM NaCl, 10% glycerol, 1 mM EDTA, 2 mM EGTA, 1 mM DTT, 5 mM Na<sub>3</sub>VO<sub>4</sub>, 5 mM NaF, 1 mM AEBSF, aprotinin (5  $\mu$ g/ml), and leupeptin (5  $\mu$ g/ml). Cell debris and nuclei were removed by centrifugation at 15,000 g for 10 min and the protein concentration was determined by Bradford assay (Pierce). The clarified cell lysates were mixed with 5x SDS sample buffer and boiled for 5 min at 94 °C. The proteins were separated by SDS-PAGE and then transferred onto nitrocellulose membranes by electroblotting for 2 h at constant 80 voltage. The membranes were blocked with 5% bovine serum albumin (BSA) or 5% dry skim milk in Tris-buffered saline containing 0.05% (v/v) Tween-20 (TBST) for 1 h and then incubated at 4 °C overnight with the indicated antibody in a blocking buffer. After washing three times with TBST, membranes were incubated with a horseradish peroxidase-conjugated secondary antibody (Amersham Biosciences) in a blocking buffer. The immune-reactive bands were detected with an enhanced chemiluminescence kit (AbFrontier, Korea) and quantified by a ChemiDoc Touch imaging system (Bio-Rad, USA).

For immunoprecipitation experiment, cells were stimulated with or without 100  $\mu$ M H<sub>2</sub>O<sub>2</sub> for the indicated times, rinsed once with cold PBS, and lysed in a lysis buffer. The cell lysates were pre-cleared with 10  $\mu$ l of protein A/G agarose beads (Amersham Biosciences) for 1 h. The cleared lysates were incubated with either 2  $\mu$ g of IKK $\gamma$  antibodies for 4 h and mixed with 20  $\mu$ l of protein A/G agarose beads or 25  $\mu$ l of anti-Flag (M2) affinity Gel (Sigma-Aldrich). The lysates were further rotated overnight at 4 °C. The beads were washed three times with 1 ml of lysis buffer. The final protein precipitates were subjected to immunoblot analyses.

## 2.8. In vitro kinase assay

The IKK complexes, p38 MAPK, and MK2 kinases were immunoprecipitated by incubating with 2  $\mu$ g of anti-IKK $\gamma$  (FL-419), anti-phospho-p38, and anti-phospho-MK2 antibodies, respectively, for 3 h followed by mixing with 20  $\mu$ l of protein A/G agarose beads. The beads were washed twice with a lysis buffer and further twice with a kinase buffer (20 mM HEPES (pH 7.4), 5 mM MgCl<sub>2</sub>, 10 mM  $\beta$ -glycerolphosphate, 1 mM Na<sub>3</sub>VO<sub>4</sub>, 2 mM NaF, and 1 mM dithiothreitol). Then, the kinase-bound beads were incubated in 40  $\mu$ l of a kinase buffer

containing 10  $\mu$ M ATP, 1  $\mu$ Ci [ $\gamma$ -<sup>32</sup>P] ATP, and either 2  $\mu$ g or 10  $\mu$ g of substrate proteins (GST- $\kappa$ B (1–54) for IKK, myelin basic protein (MBP) and GST-MFF1 for p38 and MK2 kinases) at 30 °C for 30 min. The reaction was stopped by adding 10  $\mu$ l of 5  $\times$  SDS sample buffer. After boiling, half of reaction mixture was resolved on a 10% denaturing gel and subjected to autoradiography; the other half of reaction mixture was used for immunoblotting the kinase proteins.

## 2.9. Immunofluorescence staining

HeLa cells were cultured on a slide glass and stimulated with H<sub>2</sub>O<sub>2</sub>. The cells were fixed with 4% paraformaldehyde. After washing with cold PBS, the fixed cells were permeabilized by incubating with a blocking solution containing 3% BSA and 0.2% Triton X-100 in PBS for 15 min. Subsequently, the fixed cells were incubated at 4 °C overnight with anti-p65 antibody (1:500, Santa Cruz) in the blocking solution and then with a secondary antibody (Donkey anti-mouse IgG antibody conjugated with Alexa Fluor 568 at 1:250 dilution, ThermoFisher Scientific) for 30 min at RT. Nuclei were labeled with DAPI. Fluorescent signals were taken using a LSM880 laser scanning confocal microscope (Carl Zeiss) equipped in the Fluorescence Core Imaging Center (Seoul, Korea). Intensities of captured images were quantified using ImageJ software (NIH).

## 2.10. Live cell microscopic imaging

For HSP60 release, HeLa Cells were plated at a density of 2  $\times$  10<sup>4</sup> cells/well of 12-well plates and transfected with pcDNA3-MTS-EGFP-PH-HSP60 plasmids using turbofect transfection reagents (ThermoFisher Scientific). After 24 h transfection, plasma membrane was stained using CellMask Deep Red (1:1000, ThermoFisher Scientific) for 10 min at 37 °C. Then, cells were washed twice with PBS and treated with 20 mU of glucose oxidase (GOx). Fluorescence signals were detected by a Nikon A1R microscope R microscope. Images were visualized using NIS-Elements software (Nikon, Japan).

For mitochondrial membrane potential, live cell imaging was performed in an inverted fluorescence microscope (Zeiss) equipped with CoolLED (pE-2) as a light source. Cells were stained with 20 nM tetramethylrhodamine ethyl ester TMRE (Invitrogen, USA) for 20 min at 25 °C. Time-lapse imaging was obtained in a 5-min interval for 1 h by using Metamorph imaging program (Molecular devices, USA). Fluorescence intensities were quantified using imageJ software.

Level of mitochondrial oxidation was measured using a GPD-roGFP ratiometric redox sensor targeted mitochondrial intermembrane space. Fluorescence images were taken by a confocal microscope (Leica) with two excitation filter (405 nm, 488 nm) and emission filter (493–533 nm) in a ratio mode.

Intracellular ROS generation was assessed using 5, 6-chloromethyl-2', 7'-dichlorodihydrofluorescein diacetate (CM-H<sub>2</sub>DCFDA). The cells (2  $\times$  10<sup>5</sup>) were plated on 35-mm dishes and cultured for 24 h. Cells were incubated in the hypoxic chamber for 4 h and returned to the normoxic condition for 15 min. Then, cells were rinsed once with ice-chilled KREB's Ringer solution and incubated for 5 min with 5  $\mu$ M CM-H<sub>2</sub>DCFDA. The DCF fluorescence images were immediately acquired by fluorescence microscopy (Axiovert200, Zeiss). The fluorescence intensities were quantified and averaged from 80 to 100 cells using an ImageJ system.

## 2.11. Proximity ligation assay

HeLa cells were grown on a glass cover for 12 h and then stimulated with H<sub>2</sub>O<sub>2</sub> for indicated times. After stimulation, cells were rinsed twice with cold PBS and then fixed with 3.7% paraformaldehyde for 10 min. The fixed cells were permeabilized with 0.1% Triton X-100 in PBS for 5 min and incubated with a drop of blocking buffer for 30 min at 37 °C. The plus and minus antibodies (1:100 for  $\alpha$ -VDAC1, 1:150 for  $\alpha$ -ANT2,

1:250 for  $\alpha$ -HSP60, 1:250 for  $\alpha$ -IKK $\beta$ , and 1:250 for  $\alpha$ -IKK $\gamma$  antibodies) were diluted in blocking buffer containing  $1 \times$  Duolink assay reagent (Sigma-Aldrich) and incubated with the samples overnight at 4 °C. The polymerase chain reaction was performed according to the manufacturer's instructions. After the polymerase chain reaction, nuclei were stained with DAPI for 10 min at room temperature. Images were taken using a Zeiss LSM 880 confocal microscope.

### 2.12. Chemical cross-linking experiment

Cells were stimulated with or without 100  $\mu$ M of H<sub>2</sub>O<sub>2</sub> for 4 h. Then, the cells were incubated with 200  $\mu$ M of 1,5-difluoro-2,4-dinitrobenzene (DFDNB) as a cross-linking reagent for 30 min at 30 °C. After cross-linking, cells were lysed by a lysis buffer and subjected to SDS/PAGE and immunoblotting with anti-VDAC1 antibody.

### 2.13. NF- $\kappa$ B reporter assay

HeLa cells were co-transfected with a NF- $\kappa$ B-luciferase reporter plasmid (Stratagene) and pRV-SV40 control plasmid for 24 h. After transfection, the cells were incubated with or without 100  $\mu$ M of H<sub>2</sub>O<sub>2</sub> for 6 h. The luciferase activities were measured by dual luciferase assay kit (Promega).

### 2.14. RNA-seq analysis

RNA sequencing data were produced on the Illumina NovaSeq platform with 100 bp paired-end reads. Raw data were trimmed by Sickle (ver. 1.33) for quality control (QS > 20). STAR-RSEM pipeline was used for read alignment to the hg19 reference genome and for expression quantification at the gene level. We removed the low expressed genes with CPM < 1 in more than a third of samples for each cell line. Differentially expressed genes (DEGs) were computed using edgeR (ver. 3.26.5) with FDR < 0.05 for OS-induced genes and with p-value < 0.05 for down-regulated genes by HSP60 N antibody treatment. Transcription factor binding analysis was achieved using oPOSSUM 3.0. The JASPAR core profile for NF- $\kappa$ B was used to scan promoter regions defined as -5000 bp to +2000 bp from the transcription start site of DEGs. All 24,752 genes in oPOSSUM were used as background signal and the hits with the matrix score > 85% and conservation score > 0.40 were considered to be positive. The mRNA sequencing data were submitted to the GEO repository.

### 2.15. Hypoxia-reoxygenation experiment

HeLa cells were incubated under either hypoxia (0.1% or 2% O<sub>2</sub>) condition for 4 h. Then, the cells were returned to normoxic (20% O<sub>2</sub>) condition for reoxygenation. Control cells were left under normoxic condition for 4 h. The establishment of hypoxia and anoxia was confirmed by immunoblotting HIF-1 level.

### 2.16. Tumor xenograft model

All mouse experiments were approved by the Institutional Animal Care and Use Committee (IACUC) of Ewha Womans University, South Korea, and conformed to the ARRIVE guidelines. HeLa-Luc cells (PerkinElmer) stably expressing either WT or D423A mutant of cytosol-targeted HSP60 ( $2 \times 10^6$  cells) were suspended in 100  $\mu$ l of Matrigel solution (BD Biosciences) and subcutaneously injected into 5-week-old male mice. Measurement of tumor volume was performed once every three days by the 2D optical topography. Briefly, the mice were intraperitoneally injected with D-luciferin solution (150 mg/kg, Caliper Life Sciences), anesthetized with 2% isoflurane after 10 min, and then imaged for 10 s using IVIS 200 system (Xenogen). Tumor tissues were removed and weighed at 4 weeks post cell implantation.

### 2.17. Statistical analysis

The data were analyzed with either Student's t-test for comparisons between two groups or two-way ANOVA with Tukey HSD post hoc test for multiple groups containing two variables (GraphPad 5.0). P-value of less than 0.05 was considered significant.

## 3. Results

### 3.1. Mild OS induces the selective release of HSP60 from mitochondria

To assess how mammalian cells respond to the differential strength of external OS, we challenged HeLa cells with differential OS levels by increasing concentration of H<sub>2</sub>O<sub>2</sub>. The viability assay showed that HeLa cells were alive at the concentrations below 200  $\mu$ M H<sub>2</sub>O<sub>2</sub>, but all dead at the concentrations above 1 mM H<sub>2</sub>O<sub>2</sub> (Fig. 1A). When the cellular ATP level was measured as an indicator of cellular homeostasis, treatment with 100  $\mu$ M H<sub>2</sub>O<sub>2</sub> (hereafter referred to as "mild OS") transiently reduced the cellular ATP level, which later boosted to the higher level than that in normal cells (Fig. 1B). In contrast, treatment with 1 mM H<sub>2</sub>O<sub>2</sub> (hereafter referred to "severe OS") drastically decreased the cellular ATP level to the zero, which could no longer be recovered, indicating irreversible cellular damage and death. To further assess the mitochondrial integrity, the transmembrane potential ( $\Delta\psi_m$ ) was measured using tetramethylrhodamine ethyl ester. Fluorescence imaging analysis showed that OS rapidly induced the transmembrane potential dissipation and recovery was observed only in the case of mild OS (Supplementary Fig. 1A). In addition, the immunofluorescence staining of cytochrome c indicated that mild OS somewhat triggered the mitochondrial fission process at the kinetics similar to those observed in the case of ATP change, meaning that the mitochondrial functional recovery occurred in a reversible manner (Supplementary Fig. 1B). Altogether, our results show that mild OS induces a change in mitochondrial function that can be recovered, while severe OS causes the irreversible mitochondrial damage.

Next, we examined the subcellular compartments in the H<sub>2</sub>O<sub>2</sub>-treated HeLa cells to identify a protein signature responding to differential OS level. Unexpectedly, we noticed an increase of mitochondrial matrix protein HSP60 in the cytosolic fraction. Quantitative analysis of immunoblots indicated that the basal level of HSP60 in cytosol started at approximately 0.5% of its level in mitochondria and increased up to 3.5% by treatment with mild OS (Fig. 1C). The cytosolic level of HSP60 was also increased by mild OS in a timely manner (Supplementary Fig. 2A). Moreover, it should be noted that peroxiredoxin (Prx) type III (Prx III), which is one of the most abundant mitochondrial matrix proteins, was not appeared in the cytosolic fraction of mild OS-treated cells. The fact that Prx III (25 kDa) is smaller in size than HSP60 supported the idea that the increase in cytosolic HSP60 level is a selective process. Moreover, the cytochrome c was retained in the mitochondria under the mild OS conditions and was completely released into the cytosol under severe OS conditions, which precisely correlates with the severe OS-induced cell death. Further subcellular fractionation experiments showed that mild OS-induced increase of the HSP60 level in the cytosolic fraction was broadly detected among various tissue-origin cell types, such as HepG2 (liver), HCT116 (colon), and MDA-MB-231 (breast) (Fig. 1D). Alternatively, the artificial agents capable of generating cytosolic OS, such as the GSH-depleting diamide and the herbicide paraquat, also induced an increase in cytosolic HSP60 level (Supplementary Figs. 2B and C). We further examined the effect of mild and persistent OS challenge on the cytosolic HSP60 level. To do so, we employed glucose oxidase (GOx) that steadily generates H<sub>2</sub>O<sub>2</sub> in a low micromolar range (~10  $\mu$ M H<sub>2</sub>O<sub>2</sub>/mU enzyme). Treatment with GOx induced a marked increment in cytosolic HSP60 level in a dose-dependent manner (Fig. 1E). In addition, we addressed whether external OS affects the intra-mitochondrial ROS level. A thiol-based ratiometric redox sensor targeting to the mitochondrial

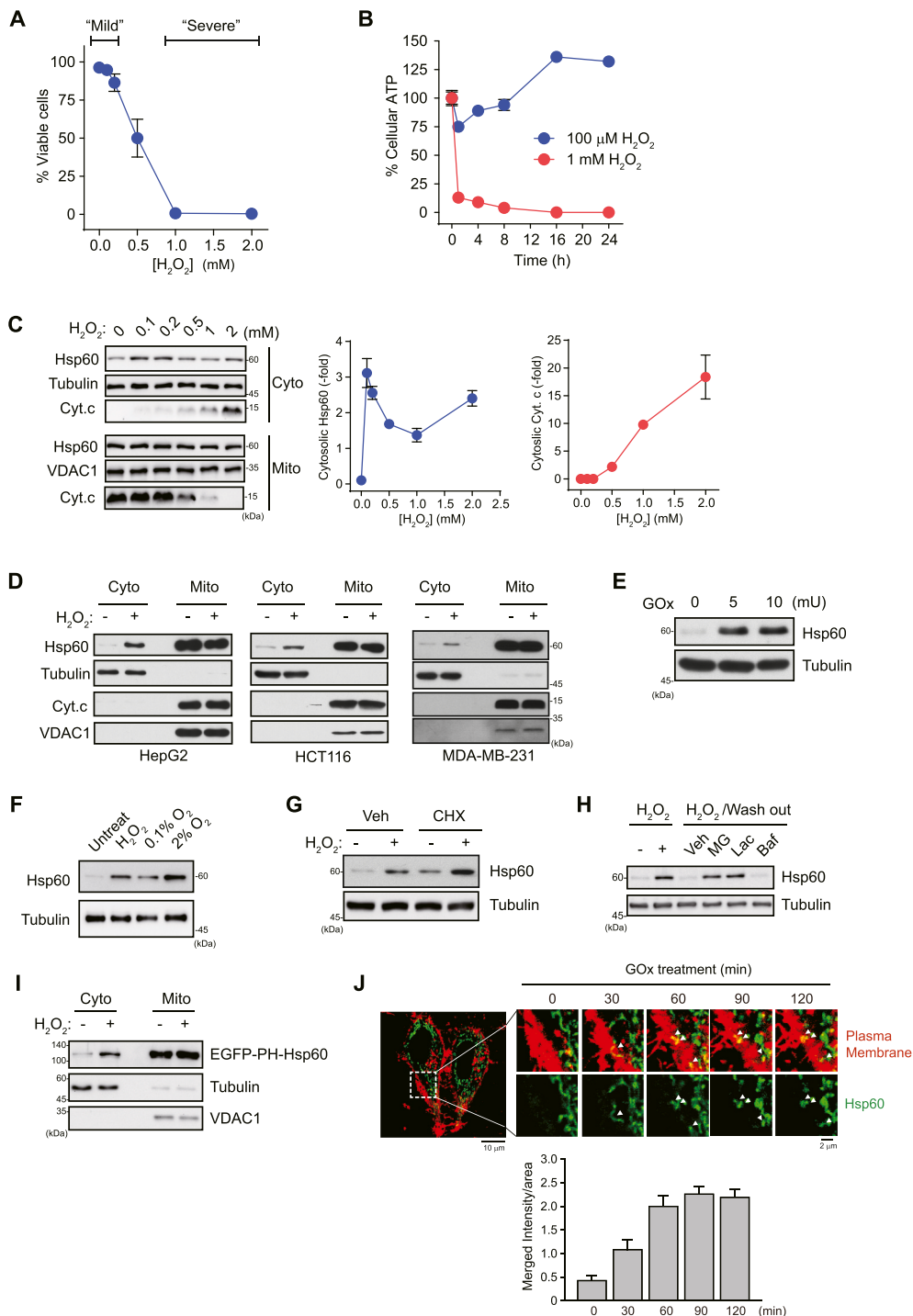


**Fig. 1.** HSP60 is released from mitochondria. (A) HeLa cells were stimulated with increasing concentrations of H<sub>2</sub>O<sub>2</sub> for 12 h and subjected to the cell viability assay. Data in the graph are means ± SD of percent of viable cells ( $n = 3$ ). The ranges for mild and severe OS are designated. (B) HeLa cells were stimulated with 100 μM or 1 mM H<sub>2</sub>O<sub>2</sub> for indicated times and subjected to the luminescent ATP determination assay. Data in the graph are means ± SD of percent of cellular ATP level versus unstimulated sample ( $n = 3$ ). (C) HeLa cells were stimulated with increasing concentrations of H<sub>2</sub>O<sub>2</sub> for 4 h. Subcellular fractions were immunoblotted. The immune bands for HSP60 and cytochrome c were quantified and normalized by the intensity of α-tubulin bands. Data in the graph are means ± SD of relative band intensities ( $n = 3$ ). VDAC1 and α-tubulin are mitochondrial and cytosolic markers, respectively. (D) HepG2, HCT116, and MDA-MB-231 cells were stimulated with 100 μM H<sub>2</sub>O<sub>2</sub> for 4 h. Cytosolic (Cyto) and mitochondrial (Mito) fractions were immunoblotted. (E) HeLa cells were treated with glucose oxidase (GOx) at the indicated units. Cytosolic fractions were immunoblotted. (F) HeLa cells were kept in the hypoxia conditions (0.1% and 2% O<sub>2</sub> level) for 4 h and then reoxygenated for additional 4 h in the normoxia condition. Cytosolic fractions were prepared and immunoblotted ( $n = 3$ ). Stimulation with 100 μM H<sub>2</sub>O<sub>2</sub> was a positive control. (G) HeLa cells were stimulated with 100 μM H<sub>2</sub>O<sub>2</sub> for 4 h in the presence or absence of cycloheximide (CHX). Cytosolic fractions were immunoblotted. Vehicle control (Veh) is 0.1% DMSO. (H) HeLa cells were stimulated with 100 μM H<sub>2</sub>O<sub>2</sub> for 4 h, rinsed with fresh media, and further cultured for 1 h. Cytosolic fractions were immunoblotted. Cell lysates from HeLa cells stimulated with or without 100 μM H<sub>2</sub>O<sub>2</sub> for 4 h are loaded as positive controls. Vehicle control (Veh) is 0.1% DMSO. MG, MG132. Lac, lactacystin. Baf, bafilomycin A1. (I) HeLa cells expressing the EGFP-PH-HSP60 fusion proteins were stimulated with or without 100 μM H<sub>2</sub>O<sub>2</sub> for 4 h. Subcellular fractions were immunoblotted. VDAC1 and α-tubulin are mitochondrial and cytosolic markers, respectively. (J) Time-lapse live-cell images were taken from HeLa cells expressing the EGFP-PH-HSP60 fusion proteins after GOx (20 mU) was treated. Plasma membranes were stained with a CellMask Deep Red. Merged patches (yellow) indicated by arrowheads were quantified. Data in the graph are means ± SD of fluorescence intensity of merged patches per membrane area (μm<sup>2</sup>). A representative image is shown ( $n = 3$ ). Dashed box in the low power field (Left) indicates the zoom-in area. Immunoblot (IB)

shown is a representative of three independent experiments. See also [Supplementary Figs. 1–S3](#). (For interpretation of the references to colour in this figure legend, the reader is referred to the Web version of this article.)

intermembrane space, named IMS-roGFP [17], indicated that mild OS did not change the ROS level inside mitochondria, whereas severe OS significantly increased ROS levels ([Supplementary Fig. 2D](#)). Consistently, the mitochondria ROS increased by rotenone and mito-paraquat

did not change the cytosolic HSP60 level ([Supplementary Figs. 2C and E](#)). Moreover, the targeted overexpression of catalase in mitochondria, which led to the elimination of mitochondrial H<sub>2</sub>O<sub>2</sub> [18], did not affect the cytosolic HSP60 level increased by mild OS ([Supplementary Fig. 2F](#)).

Based on these additional experiments, we excluded the possibility of involvement of intra-mitochondrial ROS. Finally, we tested the hypoxia/reoxygenation (H/R) injury as a physiological OS model. Indeed, the H/R condition increased the intracellular ROS level as well as the cytosolic HSP60 level (Supplementary Fig. 2G and Fig. 1F). Overall, our data demonstrate that the increase in cytosolic HSP60 level in response to mild OS is likely a well-conserved mechanism.

Next, we investigated the origin of cytosolic HSP60 responding to mild OS. The pretreatment of a translation inhibitor, cycloheximide, did not inhibit the increase in cytosolic HSP60 by mild OS (Fig. 1G), which led us to exclude the new protein synthesis. When H<sub>2</sub>O<sub>2</sub> was washed out following 1-h treatment, the cytosolic HSP60 disappeared by

proteasomal, not lysosomal, degradation (Fig. 1H), which implicates a rapid turnover of HSP60 in cytosol. From these results, we postulated that the cytosolic HSP60 could be originating in the mitochondria. To trace the mitochondrial release of HSP60 in a live cell, we designed a fluorescent reporter where the enhanced green fluorescence protein (EGFP) and phospholipase C  $\delta$ 1-pleckstrin homology (PH) domain are inserted in tandem, following the mitochondrial targeting signal (MTS), in the HSP60 open reading frame (Supplementary Fig. 3A). The PH domain directs the plasma membrane anchoring of a reporter protein via phosphoinositide binding [19]. The expression level of EGFP-PH-HSP60 reporter was much lower than that of the endogenous HSP60, but this level was sufficient for analyzing an unequivocal localization of the

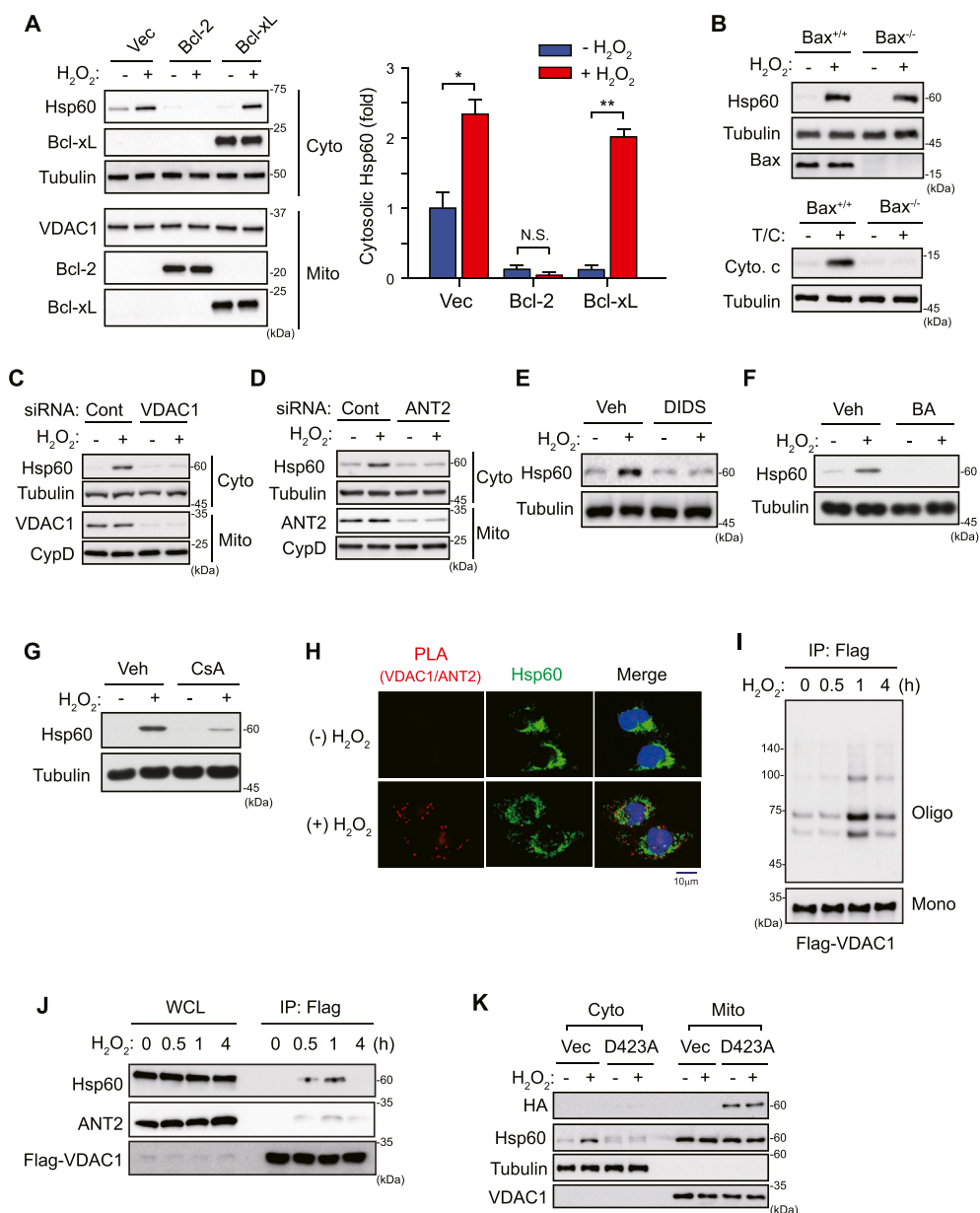


**Fig. 2.** HSP60 release requires the VDAC1 oligomerization.

(A) HeLa cells expressing Bcl-2 or Bcl-X<sub>L</sub> were stimulated with 100  $\mu$ M H<sub>2</sub>O<sub>2</sub> for 4 h. Subcellular fractions were immunoblotted. The immune bands for HSP60 were quantified and normalized by the intensity of  $\alpha$ -tubulin bands. Data in the graph are means  $\pm$  SD of relative band intensities ( $n = 3$ , \* $P < 0.002$ , \*\* $P < 0.001$ ). VDAC1 and  $\alpha$ -tubulin are mitochondrial and cytosolic markers, respectively. N.S., not significant. (B) Bax<sup>+/+</sup> and Bax<sup>-/-</sup> HCT116 cells were stimulated with either 100  $\mu$ M H<sub>2</sub>O<sub>2</sub> for 4 h or TNF- $\alpha$ /CHX for 4 h. Cytosolic fractions were immunoblotted for HSP60, Cytochrome c (Cyto. c), and  $\alpha$ -tubulin. Total cell lysates were used for immunoblotting Bax protein. (C and D) The siRNA-transfected HeLa cells stimulated with 100  $\mu$ M H<sub>2</sub>O<sub>2</sub> for 4 h. Subcellular fractions were immunoblotted. Firefly luciferase siRNA is used for control (Cont). (E–G) HeLa cells were pretreated with indicated inhibitors for 1 h and then stimulated with 100  $\mu$ M H<sub>2</sub>O<sub>2</sub> for 4 h. Cytosolic fractions were immunoblotted. Vehicle control (Veh) is 0.1% DMSO, 4,4'-diisothiocyanostilbene-2,2'-disulfonic acid (DIDS), 25  $\mu$ M; bongkreikic acid (BA), 10  $\mu$ M; cyclosporin A (CsA), 0.5  $\mu$ M. (H) HeLa cells were stimulated with 100  $\mu$ M H<sub>2</sub>O<sub>2</sub> for 4 h and subjected to the proximity ligation assay (PLA) for VDAC1 and ANT2. Representative images are shown ( $n = 3$ ). Mitochondria and nuclei were stained with anti-HSP60 antibody and DAPI, respectively. (I) HeLa cells were transfected with a plasmid encoding Flag-tagged human VDAC1 and stimulated with 100  $\mu$ M H<sub>2</sub>O<sub>2</sub> for indicated times. Cells were lysed in a lysis buffer containing a chemical cross-linker, 1,5-difluoro-2,4-dinitrobenzene (BFDNB), and then subjected to the immunoprecipitation with anti-Flag antibody (M2). VDAC1 was immunoblotted by HRP-conjugated M2 antibody. (J) HeLa cells were transfected with the plasmids encoding Flag-tagged VDAC1 and stimulated with 100  $\mu$ M H<sub>2</sub>O<sub>2</sub> for indicated times. Cell lysates were subjected to the immunoprecipitation with M2 antibody. HSP60 and ANT2 were immunoblotted. Total cell lysate was loaded for control. (K) HeLa cells were transfected with either control vector (Vec) or plasmids encoding an ATP binding-defective mutant of full-length HSP60 (D423A) with hemagglutinin (HA) tag. The transfected cells were stimulated with 100  $\mu$ M H<sub>2</sub>O<sub>2</sub> for 2 h. Subcellular fractions were immunoblotted (IB). VDAC1 and  $\alpha$ -tubulin are mitochondrial and cytosolic markers, respectively. Immunoblot (IB) shown is a representative of three independent experiments.

fluorescent reporter to the mitochondria by microscopic imaging (Supplementary Figs. 3B and C). Moreover, the immunoblot analysis demonstrated that mild OS increased the cytosolic levels of EGFP-PH-HSP60 reporter and endogenous HSP60 (Fig. 1I). Then, we performed the live cell confocal imaging of the EGFP-PH-HSP60 reporter in HeLa cells, whose plasma membranes were pre-labeled with red-fluorescent lipophilic probe. Strikingly, the time-lapse imaging revealed that the yellow scattered patches resulting from merging of the green reporter proteins with red membrane probes began to appear at 30 min and further increased after GOx treatment (Fig. 1J). Alternatively, when the EGFP-PH-HSP60 reporter was co-expressed with a red fluorescent protein (RFP)-PH reporter (Supplementary Fig. 3D), the quantification of snap-shot fluorescence images revealed that the fraction of HeLa cells showing the co-localization of EGFP-PH-HSP60 and RFP-PH reporters was markedly increased by mild OS ( $14.5 \pm 2.6\%$  and  $70.6 \pm 6.8\%$  in the control and  $\text{H}_2\text{O}_2$ -stimulated samples, respectively). Collectively, the microscopic analyses using reporter constructs firmly supports that mitochondrial HSP60 was released into the cytosol under mild OS condition.

### 3.2. HSP60 is released through the VDAC1-centered membrane pore

Mitochondrial proteins can be liberated via the transmembrane macropores, such as the Bax/Bak macropore that causes mitochondrial outer membrane permeabilization (MOMP) [20] or the VDAC1-dependent mitochondrial permeability transition (mPT) complex that penetrates outer and inner membranes [21]. Because the Bcl-2 family proteins are the master regulator of mitochondrial membrane pores [22], the HSP60 release was tested in HeLa cells stably expressing either Bcl-2 or Bcl-X<sub>L</sub> proteins. Western blot analyses of subcellular fractions showed that the expression of Bcl-2, not Bcl-xL, markedly diminished the HSP60 release induced by mild OS (Fig. 2A), which suggests that HSP60 is released probably through a selective mitochondrial membrane pore.

To identify the components of mitochondrial membrane pore involved in the HSP60 release, we first tested the Bax/Bak macropore using the Bax-proficient and -deficient HCT116 cell lines. Western blot analysis of cytosolic fractions confirmed that Bax is required for the release of cytochrome *c* by the stimulation of apoptosis but is not involved in the HSP60 release induced by mild OS (Fig. 2B). Next, we addressed whether the VDAC1-dependent mPT complex is involved in the HSP60 release. The mPT complex contains three major components, voltage-dependent anion channel 1 (VDAC1) in outer mitochondrial membrane, adenine nucleotide translocase 2 (ANT2) in inner mitochondrial membrane, and cyclophilin D in matrix [3]. Thus, we examined the involvement of each component in the OS-induced HSP60 release. Surprisingly, the genetic ablation and chemical inhibition of VDAC1 as well as ANT2 inhibited the release of HSP60 induced by mild OS (Fig. 2C–F). More importantly, cyclosporine A (CsA) that inhibits cyclophilin D as a key regulator of mitochondrial function also reduced the OS-induced HSP60 release (Fig. 2G). To investigate the constitution of membrane pore complex under mild OS, we performed a proximity ligation assay (PLA) capable of detecting single protein-protein interactions *in situ* [23]. Indeed, microscopic images showed that mild OS induced proximal association between VDAC1 and ANT2 in the mitochondrial outer and inner membranes respectively (Fig. 2H). Moreover, chemical cross-linking experiments revealed that VDAC1 were oligomerized to the high molecular weight under mild OS (Fig. 2I). Co-immunoprecipitation experiment showed that the oligomeric VDAC1 complex induced by mild OS comprised both HSP60 and ANT2 (Fig. 2J). Such biochemical studies suggest that HSP60 traverses the VDAC1-centered pore complex.

Because HSP60 is located in the mitochondrial matrix as an oligomeric chaperone complex [10], we investigated how HSP60 penetrates the membrane pore. Size-exclusion chromatography showed that the mild OS induced the structural transition of HSP60 proteins from

oligomers to monomers (Supplementary Fig. 4). This result is consistent with that of a previous physicochemical study indicating that the HSP60 proteins undergo a dynamic structural transition between oligomers and monomers depending on the ATP binding [24]. Thus, we studied the HSP60 release in the HeLa cells stably expressing an HSP60 mutant (D423A) that lacks ATP-binding activity. Of note, the immunoblot analysis of subcellular fractions revealed that the expression of D423A mutant prevented the release of not only endogenous HSP60 but also the mutant itself under mild OS (Fig. 2K). This simple experiment indicates that the ATP binding of HSP60 is essential for its release from mitochondria; in addition, the D423A mutant is likely to act as a dominant negative mutant interfering with the release of endogenous HSP60. Collectively, our results demonstrated that VDAC1 organizes the formation of an unprecedented membrane pore complex to mediate the retrograde liberation of a monomeric HSP60 into cytosol.

### 3.3. Activation of p38 MAPK is a key cytosolic signaling event for HSP60 release

To identify the signaling pathway activating the mild OS-induced VDAC1 oligomerization, we screened various OS-responsive protein kinases for the HSP60 release. As a result, mild OS induced the marked activation of only p38 MAPK in various cancer cell types (Fig. 3A), whereas severe OS activated other stress-related protein kinases, such as JNK and c-Src, (Supplementary Fig. 5A). Constantly, the p38 kinase inhibitor, SB203580, completely blocked the HSP60 release induced by mild OS (Fig. 3B), which indicated that the p38 activation is required for the HSP60 release. Subsequently, we addressed if the p38 activation associates with the mPT pore. First, the p38 kinase inhibitor prevented the dissipation of transmembrane potential ( $\Delta\psi$ ) as was observed in the case of CsA (Fig. 3C). Second, mild OS also induced the translocation of the active p38 to the mitochondria in the HeLa and HCT116 cells (Fig. 3D). Moreover, the p38 inhibition diminished the VDAC1 oligomerization (Fig. 3E). Thus, we concluded that the p38 activation is the OS-sensing signaling event for the HSP60 release.

### 3.4. P38/MK2-mediated MFF1 S155 phosphorylation induces VDAC1 oligomerization

Next, we investigated the molecular mechanism by which the p38 activation leads to the VDAC1 oligomerization. Among intracellular mitochondrial regulators associated with mPT complex, we noticed that MFF1 was recently shown to associate with VDAC1 at the outer mitochondrial membrane [25]. To assess the role of MFF1 in the HSP60 release, we chose two prostate cancer cell lines, PC3 and LNCaP, in which the levels of MFF1 proteins were quantitatively disparate and corresponded to the cytosolic HSP60 levels (Fig. 4A). Consistently, the MFF1 depletion in the PC3 cells reduced the cytosolic HSP60 level, whereas the overexpression of MFF1 in the LNCaP cells enhanced the HSP60 release in response to mild OS (Fig. 4B and C). However, it was noted that the MFF1 overexpression itself did not induce the HSP60 release, which led us to exclude the involvement of mitochondrial fission process. Subsequent co-immunoprecipitation experiment showed that MFF1 is constitutively associated with VDAC1 complex regardless of OS stimulation (Fig. 4D). This result strengthens the idea that the p38 activation may switch the MFF1-mediated HSP60 release. Because MFF1 has been shown to be a substrate of various kinases including AMPK and CK2 [26,27], we examined whether p38 kinase can phosphorylate MFF1 under mild OS. We thus performed *in vitro* kinase assay using the recombinant MFF1 proteins as substrate and found that the active p38 kinase obtained from the  $\text{H}_2\text{O}_2$ -stimulated cells markedly phosphorylated the full-length MFF1 (Fig. 4E). In contrast, the recombinant p38 enzyme (<sub>rep</sub>p38) did not phosphorylate the MFF1 protein. Because both endogenous and recombinant p38 enzymes similarly phosphorylated the general substrate myelin basic protein (MBP), it is likely that additional p38-activated MFF1 kinase is involved. Among the p38-activated

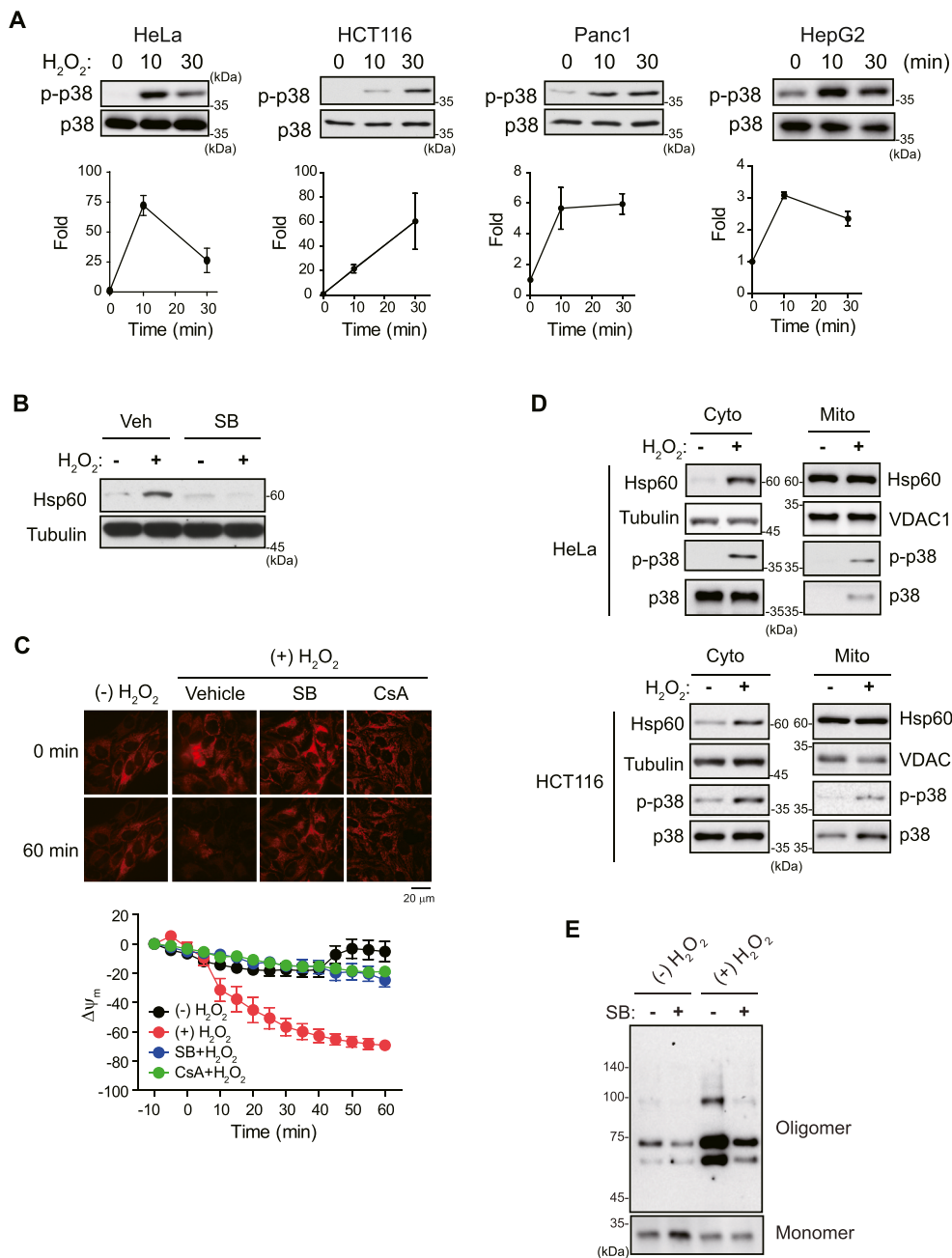


**Fig. 3.** P38 MAPK activation leads to the VDAC1 oligomerization.

(A) Four cancer cell lines were stimulated with 100  $\mu$ M H<sub>2</sub>O<sub>2</sub> for indicated times. Cell lysates were analyzed for p38 activation by phospho-specific immunoblotting. The immune bands for phosphorylated p38 were quantified and normalized by the intensity of unphosphorylated p38 bands. Data in the graph are means  $\pm$  SD of fold increases of relative band intensities ( $n = 3$ ). (B) HeLa cells were pretreated with vehicle control (0.1% DMSO) or p38 inhibitor SB203580 and then stimulated with 100  $\mu$ M H<sub>2</sub>O<sub>2</sub> for 4 h. Cytosolic fractions were immunoblotted. (C) TMRE-labeled HeLa cells were pretreated with vehicle control or inhibitors (SB203580, 10  $\mu$ M; cyclosporine A, 0.5  $\mu$ M) for 1 h. Time-lapse images were taken following treatment with or without 100  $\mu$ M H<sub>2</sub>O<sub>2</sub> for 1 h. Data in the graph are means  $\pm$  SD of transmembrane potential ( $n = 3$ ). Representative images are shown. (D) HeLa and HCT116 cells were stimulated with 100  $\mu$ M H<sub>2</sub>O<sub>2</sub> for 2 h. Sub-cellular fractions were immunoblotted. VDAC1 and  $\alpha$ -tubulin are mitochondrial and cytosolic markers, respectively. (E) HeLa cells expressing Flag-VDAC1 were treated with a p38 inhibitor for 1 h followed by 100  $\mu$ M H<sub>2</sub>O<sub>2</sub> for 2 h. The stimulated cells were incubated with a cross-linking agent BFDNB. VDAC1 was immunoprecipitated and immunoblotted with anti-Flag M2 antibody. Vehicle control (Veh) is 0.1% DMSO. Immunoblot (IB) shown is a representative of three independent experiments. See also [Supplementary Fig. 5](#).

kinases, we directly tested MK2 because it was the best-studied substrate [28]. First, the mild OS treatment induced the activation of MK2 along with p38 ([Supplementary Fig. 5B](#)). Second, the MK2 inhibitor indeed inhibited the H<sub>2</sub>O<sub>2</sub>-induced HSP60 release ([Supplementary Fig. 5C](#)). Thirdly, we confirmed the presence of MK2 in the p38 complex immunoprecipitated from the H<sub>2</sub>O<sub>2</sub>-stimulated cells ([Fig. 4E](#)). Lastly, the MK2 inhibitor completely blocked the phosphorylation of MFF1 by p38 kinase obtained from the H<sub>2</sub>O<sub>2</sub>-stimulated cells ([Fig. 4F](#)). Although AMPK has been proposed as a potential MFF1 kinase [27], we excluded its involvement because mild OS did not induce its activation and the AMPK inhibitor did not affect the HSP60 release ([Supplementary Figs. 5D and E](#)). Together, the data concluded that MFF1 is phosphorylated by p38/MK2 complex in the mild OS-stimulated cells.

To identify the potential phosphorylation site on MFF1, we performed a domain mapping study with the truncated mutants of MFF1. The *in vitro* kinase assays revealed that the amino-terminal region containing R domains likely harbors the phosphorylation sites because the

R3 domain-lacking mutant was not phosphorylated by p38 ([Fig. 4G](#)). The potential S/T residues in the R3 domain and its flanking region, including S172 AMPK substrate site, were then mutated [27]. Subsequent *in vitro* kinase assays indicated that S155 is the phosphorylation site targeted by p38/MK2 complex ([Fig. 4H](#)). Immunoblot analysis using an anti-phospho-PKD/MK2 substrate motif antibody [29] further demonstrated the endogenous phosphorylation of MFF1 WT, but not the S155A mutant, in the cells treated with mild OS ([Supplementary Figs. 5F and G](#)). Thus, the results concluded that MK2 serves as a *bona fide* MFF1 kinase. Indeed, the Ala mutation at S155, not S172, in MFF1 completely abolished the mild OS-induced VDAC1 oligomerization and HSP60 release ([Fig. 4I and J](#)). Conversely, the overexpression of a phosphomimetic S155D mutant of MFF1 triggered the HSP60 release even in the absence of mild OS ([Fig. 4K](#)). Thus, the data demonstrated that the p38/MK2-mediated phosphorylation of MFF1 at the single S155 residue proximal to the R3 domain is essential and sufficient for the HSP60 release.

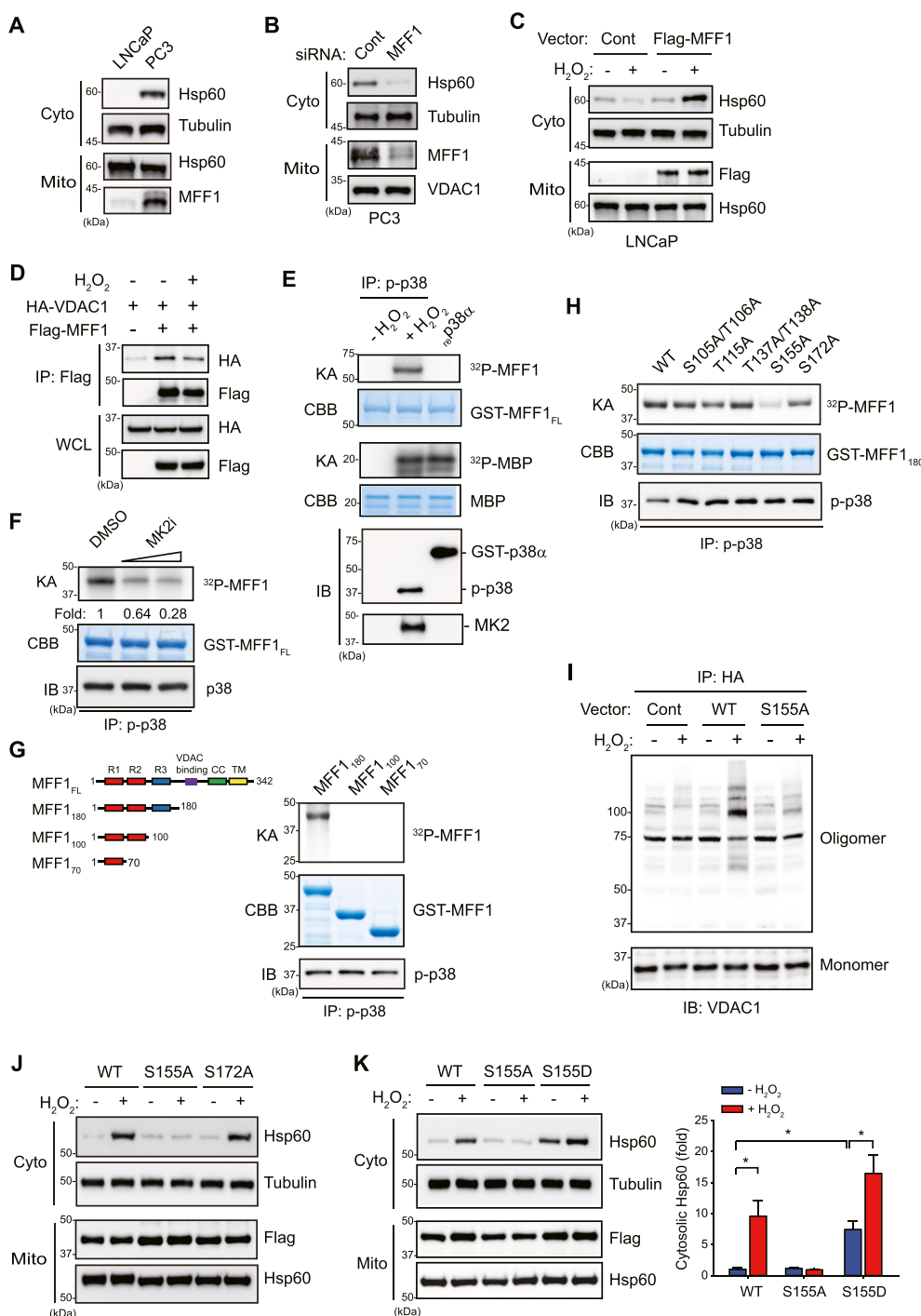


**Fig. 4.** P38/MK2-mediated MFF1 phosphorylation is a key for the HSP60 release.

(A) Subcellular fractions from two prostate cancer cell lines were immunoblotted. (B) Subcellular fractions from the siRNA-transfected PC3 cells were immunoblotted. Tubulin and VDAC1 are cytosolic and mitochondrial marker, respectively. (C) LNCaP cells were transfected with control vector or the plasmid encoding Flag-tagged MFF1 and stimulated with 100  $\mu$ M H<sub>2</sub>O<sub>2</sub> for 2 h. Subcellular fractions were immunoblotted. (D) HEK293 cells were transfected with the plasmids encoding HA-tagged VDAC1 and/or Flag-tagged MFF1 and stimulated with 100  $\mu$ M H<sub>2</sub>O<sub>2</sub> for 2 h. Cell lysates (WCL) were subjected to immunoprecipitation (IP) with anti-Flag (M2) antibody and immunoblotted for HA and Flag tags. (E–H) HeLa cells were stimulated with 100  $\mu$ M H<sub>2</sub>O<sub>2</sub> for 10 min and subjected to immunoprecipitation (IP) with anti-phospho-p38 (p-p38) antibody. The IP complexes were subjected to the kinase assay (KA) using the purified GST-fused MFF1 protein as substrate and immunoblotted with the anti-p38 or MK2 antibody. In E, recombinant GST-fused p38 enzyme (re-p38 $\alpha$ ) was directly used as a kinase source. In F, HeLa cells were pretreated with increasing concentrations of MK2 inhibitor (MK2i; 25 and 50  $\mu$ M) for 1 h. In G, truncated mutants of MFF1 are shown by schematic drawing. In H, site-directed mutants of MFF1 was used as substrate. (I–K) Effect of MFF1-S155A mutant on the VDAC1 oligomerization and HSP60 release. LNCaP cells were transfected with either control vector or the plasmids encoding FLAG-tagged MFF1 wild type (WT) and mutants and then stimulated with or without 100  $\mu$ M H<sub>2</sub>O<sub>2</sub> for 2 h. The stimulated cells were incubated with a cross-linking agent BFDNB and subjected to the immunoprecipitation (IP) and immunoblotting of HA-tagged VDAC1 (I). Subcellular fractions were immunoblotted (J and K). Data in the graph (K) are means  $\pm$  SD of fold increases of relative band intensities ( $n = 3$ ). Immunoblot (IB) shown is a representative of three independent experiments. See also [Supplementary Fig. 5](#).

### 3.5. The released HSP60 triggers IKK/NF- $\kappa$ B activation

Albeit not so strong as typical cytokine stimulations, mild OS apparently induced the activation of IKK complex in HeLa cells ([Supplementary Figs. 6A and B](#)). Thus, we studied the role of HSP60 released by mild OS in the IKK/NF- $\kappa$ B pathway. First, immunoprecipitation experiment demonstrated a transient association of HSP60 with IKK complex under mild OS in the manner that kinetically precedes the IKK activation ([Fig. 5A](#)). Second, the amount of HSP60 in the IKK complex increased by H<sub>2</sub>O<sub>2</sub> treatment at the concentration as low as 10  $\mu$ M ([Fig. 5B](#)). Third, the dynamic interaction of IKK and HSP60 in cytosol was confirmed using the PLA assay ([Fig. 5C](#)). The constitutive interaction between IKK $\beta$  and IKK $\gamma$  in the HeLa cells served as a positive control

for the PLA system. Moreover, the red-fluorescent PLA punta formed between HSP60 and IKK $\gamma$  was markedly reduced by both ANT and cyclophilin D inhibitions ([Fig. 5D](#)), strongly supporting the HSP60-releasing mechanism via the mPT complex.

To assess the signaling consequence of HSP60- $\text{IKK}$  interaction, we tested a neutralizing antibody specific to the N-terminal region of HSP60 (HSP60 N) in HeLa cells using a protein transduction method [[30](#)]. Microscopic imaging and pull-down experiment demonstrated that the HSP60 N antibody was transduced and functionally active inside cells ([Supplementary Figs. 6C and D](#)), which suggests its competence in interfering with HSP60 interaction. Indeed, the transduced HSP60 N antibody inhibited the IKK activation (e.g. serine phosphorylation and activity), the nuclear translocation of p65, and the NF- $\kappa$ B transcriptional

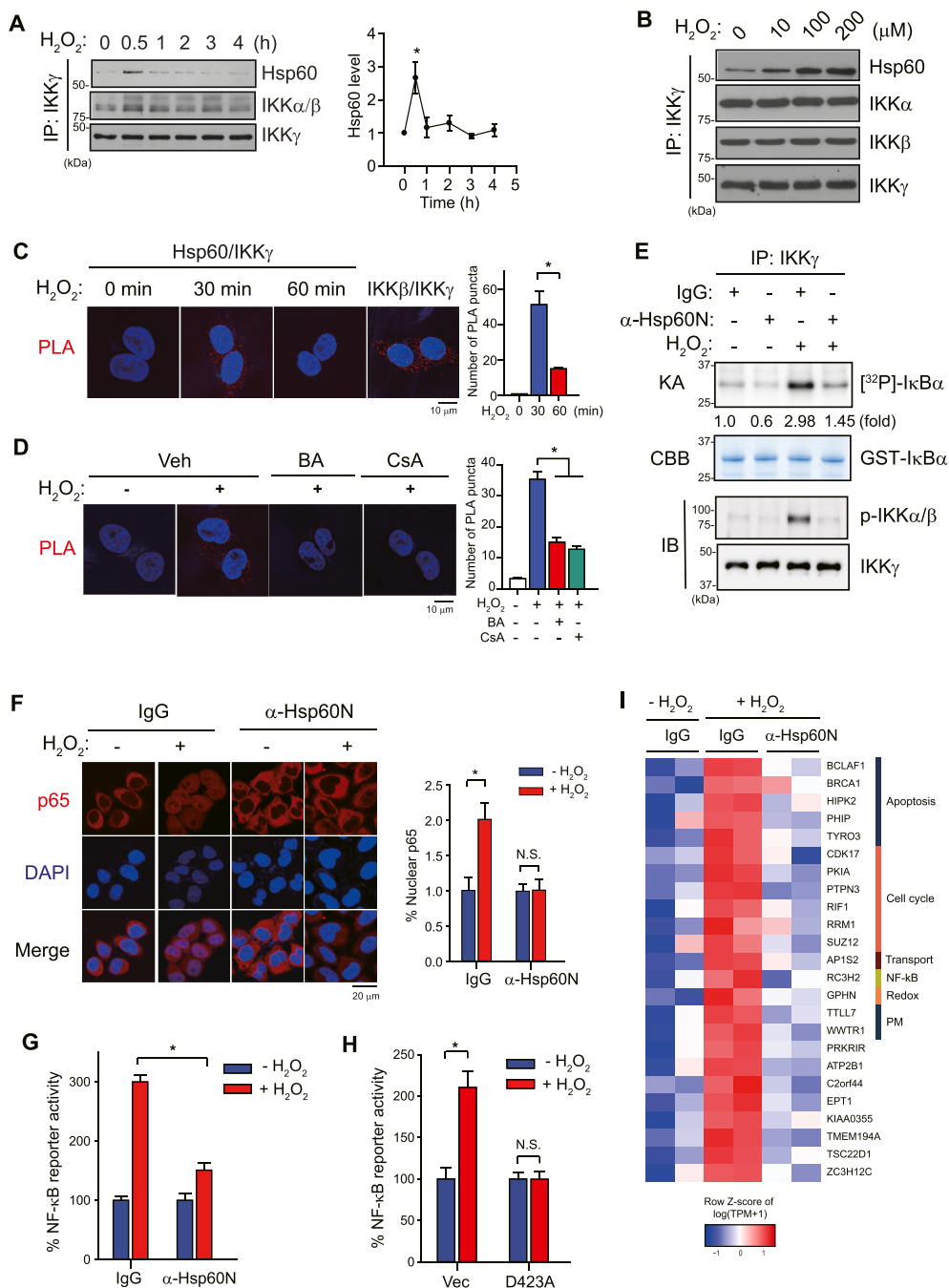


**Fig. 5.** The released HSP60 associates with and activates IkB kinase complex.

(A and B) HeLa cells were stimulated with either 100  $\mu$ M H<sub>2</sub>O<sub>2</sub> for indicated times (A) or increasing concentrations of H<sub>2</sub>O<sub>2</sub> for 30 min (B) and subjected to immunoprecipitation (IP) with anti-IKK $\gamma$  antibody. The precipitated proteins were immunoblotted (IB). In panel A, the immune bands for HSP60 were quantified and normalized by the intensity of IKK $\gamma$  bands. Data in the graph are means  $\pm$  SD of fold increases of relative band intensities ( $n = 3$ ,  $*P < 0.05$  versus unstimulated sample). Representative immunoblots are shown. (C) HeLa cells were stimulated with 100  $\mu$ M H<sub>2</sub>O<sub>2</sub> for indicated times and subjected to the proximity ligation assay (PLA) using specific antibodies against two indicated proteins. Data in the graph are means  $\pm$  SD of number of PLA puncta (red) per cell ( $n = 3$ ,  $*P < 0.01$  versus unstimulated sample). Nuclei were labeled with DAPI (blue). Constitutive interaction between IKK $\beta$  and IKK $\gamma$  is shown as a positive control. (D) HeLa cells were pretreated with indicated inhibitors for 1 h, stimulated with 100  $\mu$ M H<sub>2</sub>O<sub>2</sub> for 30 min, and subjected to the proximity ligation assay (PLA) using specific antibodies against HSP60 and IKK $\gamma$ . Data in the graph are means  $\pm$  SD of number of PLA puncta (red) per cell ( $n = 3$ ,  $*P < 0.05$  versus unstimulated sample). Nuclei were labeled with DAPI (blue). Vehicle control (Veh) is 0.1% DMSO. Bongkreic acid (BA), 10  $\mu$ M; Cyclosporin A (CsA), 0.5  $\mu$ M. (E) HeLa cells were transduced with either isotype-matched control IgG or anti-HSP60 antibody ( $\alpha$ -HSP60 N) and then subjected to the immunoblotting and *in vitro* kinase assay following stimulation with 100  $\mu$ M H<sub>2</sub>O<sub>2</sub> for 1 h. The kinase activity (KA) is expressed as means of fold increase versus unstimulated IgG-transduced sample. Representative <sup>32</sup>P- autoradiograph and coomassie brilliant blue (CBB) images are shown. (F) HeLa cells were transduced with either isotype-matched control IgG or HSP60 N antibody and stimulated with 100  $\mu$ M H<sub>2</sub>O<sub>2</sub> for 2 h. Cells were stained with anti-p65 antibody. Data in the graph are means  $\pm$  SD of fold increases of relative p65 intensities in nuclei ( $n = 3$ ,  $*P < 0.01$ ). DAPI indicates nuclei. N.S., not significant. (G and H) NF- $\kappa$ B reporter gene expression was measured in the HeLa cells either transduced with HSP60 N antibody (G) or transfected with a plasmid encoding HSP60-D423A mutant (H). Cells were stimulated with or without 100  $\mu$ M H<sub>2</sub>O<sub>2</sub> for 8 h. Data in the graphs are means  $\pm$  SD of fold increases of relative luciferase activity ( $n =$

3,  $*P < 0.001$ ). The isotype-matched IgG and empty vector were used for control. (I) Heat map depicting the significant downregulation of HSP60-dependent NF- $\kappa$ B gene expression in the MBA-MD-231 cells. Cells were transduced with either control IgG or HSP60 N antibody for 12 h and stimulated with 100  $\mu$ M H<sub>2</sub>O<sub>2</sub> for additional 8 h. Duplicate experiments are shown. PM, protein modification. See also [Supplementary Fig. 6](#). (For interpretation of the references to colour in this figure legend, the reader is referred to the Web version of this article.)

activity induced by mild OS (Fig. 5E–G). However, direct addition of the HSP60 N antibody without the transduction carrier to the culture media did not affect the p65 translocation induced by mild OS (Supplementary Fig. 6E), ruling out the presence of extracellular HSP60 as a danger signal [31]. In parallel, the expression of the release-blocking mutant of HSP60 (D423A) inhibited the mild OS-induced NF- $\kappa$ B transcription

activity (Fig. 5H).

We further conducted RNAseq analyses to examine the NF- $\kappa$ B gene expression in response to the mild OS condition. For this purpose, the MDA-MB-231 and HCT116 cells were treated with mild OS following the transduction of the isotype-matched control IgG and HSP60 N antibody. The differential gene expression (DEG) analyses yielded 105 and 183

genes ( $p$  value  $< 0.05$ ) in the MDA-MB-231 and HCT116 cells, respectively, both of which were inducible by mild OS and fully responsive to the HSP60N-mediated blockade. Subsequent transcription factor binding analysis using oPOSSUM [32] showed that 24 out of 105 DEGs ( $p$  value = 0.012) in MDA-MB-231 cells and 38 out of 183 DEGs ( $p$  value = 0.002) in HCT116 cells were predicted to be NF- $\kappa$ B target genes involved in apoptosis, cell cycle, and redox homeostasis (Fig. 5I and Supplementary Fig. 6F). Thus, this transcriptome analysis highlighted that HSP60 plays a key role in the mild OS-induced NF- $\kappa$ B gene expression for host cell survival.

### 3.6. HSP60 release confers a survival benefit in vivo

We assessed a biological significance of the HSP60-dependent regulation of NF- $\kappa$ B signaling in cellular and animal models. First, we found that transduction of HSP60 N antibody constantly aggravated the cell death in various cancer cell types treated with mild OS (Fig. 6A). Second, the expression of the release-blocking mutant (D423A) of HSP60 also enhanced the cell death in the HeLa cells treated with mild OS (Fig. 6B), and those exposed to H/R condition as physiological OS (Fig. 6C). Third, we pretreated the HeLa cells with CsA and MK2 inhibitors, both of which aggravated cell death in the HeLa cells treated with mild OS conditions (Fig. 6D and E). Lastly, overexpression of MFF1 S155A mutant also aggravated cell death in the HeLa cells treated with

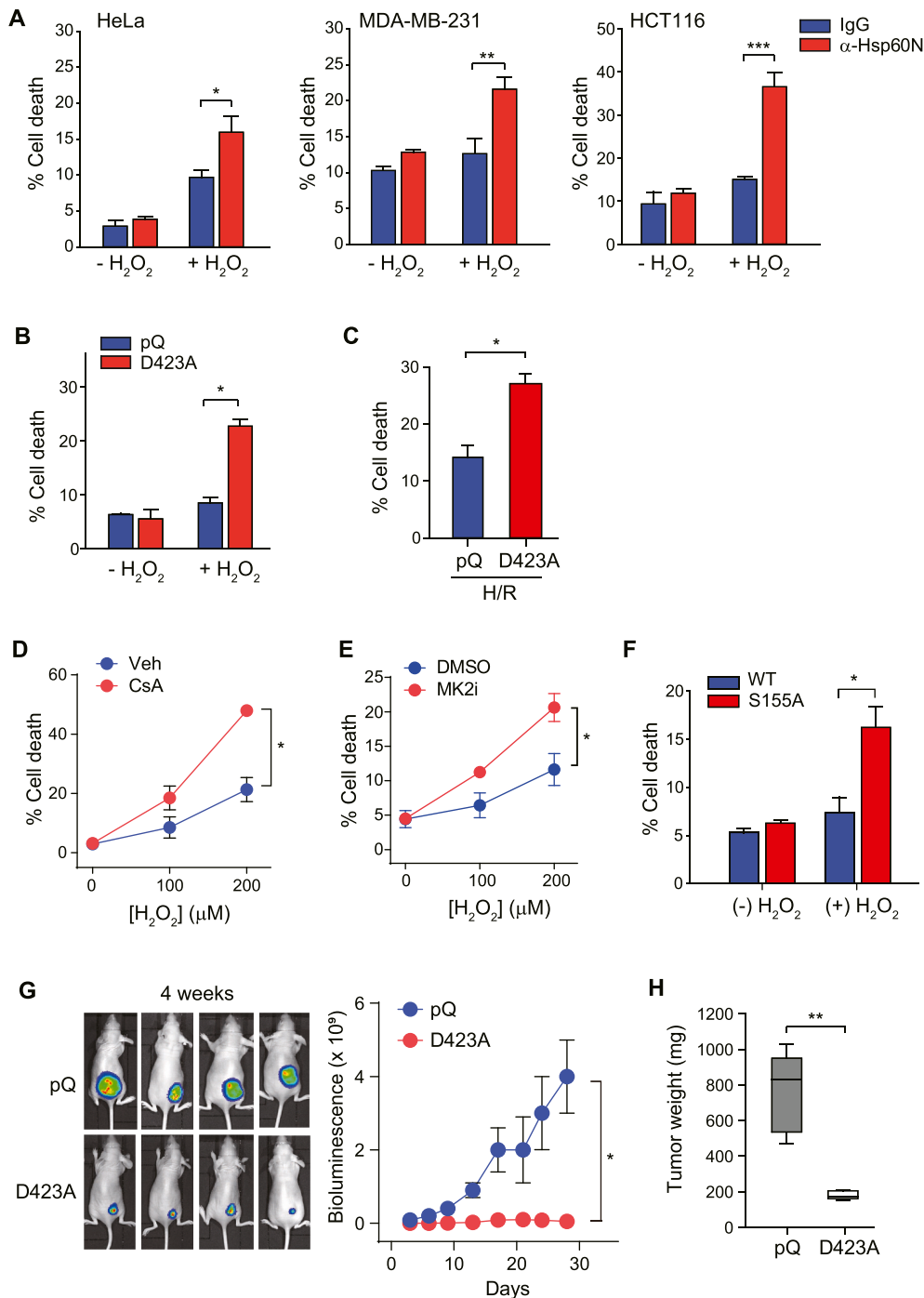


**Fig. 6.** HSP60 release promotes survivability against severe OS.

(A) Three types of cancer cells were transduced with either control IgG or HSP60 N antibody and stimulated with 100  $\mu$ M  $H_2O_2$  for 24 h. Data in the graphs are means  $\pm$  SD of percent of dead cells ( $n = 3$ , \* $P < 0.01$ , \*\* $P < 0.005$ , \*\*\* $P < 0.0005$ ). (B) HeLa cells were infected with either control retrovirus (pQ) or retrovirus encoding release-blocking mutant of HSP60 (D423A), followed by treatment with 100  $\mu$ M  $H_2O_2$  for 24 h. Data in the graphs are means  $\pm$  SD of percent of dead cells ( $n = 3$ , \* $P < 0.0001$ ). (C) HeLa cells were infected with control retrovirus (pQ) or retrovirus encoding release-blocking mutant of HSP60 (D423A) and incubated in the hypoxia/reoxygenation (H/R) condition (2%  $O_2$  for 4 h followed by reoxygenation in normoxia for 24 h). Data in the graphs are means  $\pm$  SD of percent of dead cells ( $n = 3$ , \* $P < 0.001$ ). (D) HeLa cells were pretreated with cyclosporine A (CsA, 0.5  $\mu$ M) for 1 h, followed by treatment with micromolar concentrations of  $H_2O_2$  for 24 h. Data in the graphs are means  $\pm$  SD of percent of dead cells ( $n = 3$ , \* $P < 0.001$ ). (E) HeLa cells were pretreated with the MK2 inhibitor (MK2i, 25  $\mu$ M) for 1 h, followed by treatment with micromolar concentrations of  $H_2O_2$  for 24 h. Data in the graphs are means  $\pm$  SD of percent of dead cells ( $n = 3$ , \* $P < 0.001$ ). (F) HeLa cells were infected with either control retrovirus (pQ) or retrovirus encoding MFF1 S155A mutant, followed by treatment with 100  $\mu$ M  $H_2O_2$  for 24 h. Data in the graphs are means  $\pm$  SD of percent of dead cells ( $n = 3$ , \* $P < 0.01$ ). (G and H) Release-blocking mutant of HSP60 (D423A) inhibits tumor growth *in vivo*. Growth of HeLa-Luc tumor xenograft in live mice (G) was monitored by 2D optical topography. Representative bioluminescence images obtained by IVIS *in vivo* imaging system (PerkinElmer) is shown. The excised tumors (H) was weighed at 30 day. Data in the graphs show means  $\pm$  SD of bioluminescence intensities and tumor weight ( $n = 7$  mice per group, \* $P < 0.001$ , \*\* $P < 0.0001$ ). See also Supplementary Fig. 7.

mild OS compared to that of WT (Fig. 6F). Collectively, our mechanistic evidence showed that the mitochondrial release of HSP60 is crucial for cell survival under mild OS.

We then examined whether the HSP60 release promotes cancer cell survival *in vivo* using the mouse tumor xenograft model. Cancer cells face to the pathological OS condition as the tumor-associated macrophages and neutrophils generate the robust ROS [33,34]. We performed the noninvasive bioluminescence imaging with a luciferase-expressing HeLa (HeLa-Luc) cell line stably transfected with the release-blocking mutant (D423A) of HSP60 (Supplementary Fig. 7A). The stable cells normally grew in the *in vitro* culture condition as did the parent cells. However, when the stable cells were implanted in *nu/nu* mice, the tumorigenic growth of mutant-expressing cells were impaired compared with that of the vector control cells in terms of the size and weight of tumor nodules (Fig. 6G and H; Supplementary Fig. 7B). Overall, our *in vivo* study suggests that the mitochondrial release of the mitochondrial protein HSP60 confers a survival benefit *in vivo* against pathological OS condition.

#### 4. Discussion

A vast amount of evidence has established that mitochondria release their critical components, such as cytochrome *c* and DNA, to trigger irreversible programmed cell death. By contrast, we investigated whether mitochondria rescue the damaged host cells as a beneficial endosymbiont. To this end, we thoroughly investigated the appearance of a mitochondrial protein, HSP60, in the cytosol and subsequently demonstrated that mild OS conditions trigger the mitochondrial release of HSP60 via p38/MK2-MFF1-VDAC1 axis and that the released HSP60 can activate the IKK/NF- $\kappa$ B pathway in a ligand-independent manner (Fig. 7). The pro-survival role of HSP60 in cytosol is distinct from previous mitochondria-releasing pro-apoptotic factors in that the HSP60 release is very limited in quantity and kinetically precedes the release of cytochrome *c*. Moreover, such small release of HSP60 under mild OS has

nearly no influence on the mitochondrial function and integrity and thus, likely permits immediate recovery of cellular viability. This is in stark contrast with severe OS that induces the bulk release of pro-apoptotic factor, such as cytochrome *c*, accompanied by irreversible mitochondrial dysfunction [35].

The mechanism underlying the release of mitochondrial substances has been established in the programmed cell death. For instance, cytochrome *c* and mitochondrial DNA (mtDNA) are released through the Bid/Bak/lipid supramolecular pore complex [36] and the Bax/Bak macropore [37], respectively. However, recent studies have indicated that the release of mitochondrial substances could be for the purpose of cell survival. One study demonstrated that the OS-induced VDAC polymerization induces the formation of large pore complex in the mitochondrial outer membrane, through which the mtDNA fragments are released and trigger type I interferon response for cellular recovery [38]. Other studies have reported about the release of mitochondrial protein in the integrated stress response. A mitochondrial inner membrane protein DELE1 is cleaved and released to cytosol upon mitochondrial energy stress [39,40]. Mechanistically, the released DELE1 activates eIF2 $\alpha$  kinase HRI, which induces the ATF4-dependent expression of diverse stress responsive genes that restore cellular function. Interestingly, the DELE1 release responds to neither OS nor endoplasmic reticulum stress. In the similar context, the release of mitochondrial HSP60 can be a new type of integrated stress response that defends the cells from OS. Most striking point is that a small fraction of HSP60 is released into cytosol and is sufficient to trigger the nuclear survival response via IKK/NF- $\kappa$ B pathway.

In this study, we discovered the p38/MK2-dependent phosphorylation of a mitochondrial fission receptor MFF1, specifically at the S155 site. This phosphorylation event is necessary and adequate for the VDAC1 oligomerization and the subsequent release of a pro-survival factor HSP60. Related to mitochondrial fission process, a cytosolic fission factor dynamin-related factor (Drp1) binds to R domains of the mitochondrial outer membrane receptor MFF1 [41]. Thus, it is possible

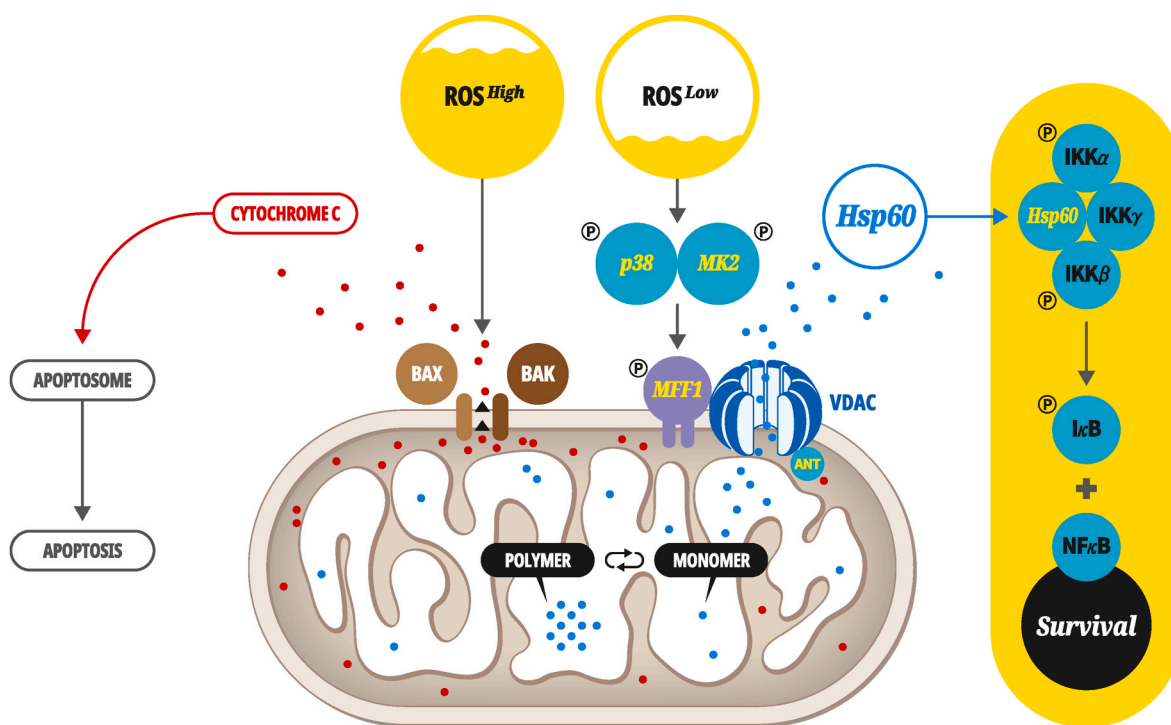


Fig. 7. Schematic model depicting the signaling mechanism underlying mitochondrial release of HSP60.

Low concentration of  $H_2O_2$ , designated by mild OS, activates p38 MAPK and MK2, which together translocate to the mitochondria and phosphorylate MFF1. The phosphorylated MFF1 directs the VDAC oligomerization. HSP60, perhaps in monomeric form, is released through the VDAC1-driven mPT complex and binds to the IKK complex in cytosol. Consequently, the activated IKK induces the NF- $\kappa$ B-dependent transcription of survival genes in the nucleus.

that the p38/MK2-mediated phosphorylation at S155 residue electrostatically prevents the Drp1 binding to the R domain. In addition, energy stresses induce mitochondrial fission through the AMPK-mediated MFF1 phosphorylation at S172 residue [27]. In this case, the p38/MK2-dependent phosphorylation of MFF1 may also interfere with the fission-associated AMPK-dependent S172 phosphorylation. Overall, the mild OS-induced p38/MK2 signaling is likely to switch the molecular function of MFF1 from mitochondrial fission to an uncharacterized VDAC1-centered mitochondrial membrane pore complex.

In summary, our study discovers an unexpected p38/MK2-mediated signaling mechanism resulting in a mito-nuclear retrograde communication that activates NF- $\kappa$ B transcription and consequently builds a survival circuit under pro-inflammatory OS. Considering that the p38/MK2 complex has been receiving great attention in reference to diverse inflammatory diseases [28,42], the mitochondrial HSP60 release can be an important downstream target for development of anti-inflammatory therapeutics based on chronic p38 MAPK/MK2 activation.

#### Author contributions

S.M. and J.K. performed most experiments; S.M. and S.W.K. designed experiments and analyzed data; H.M.C., S.P., W.S., and D.K. performed molecular imaging; H.J.Y. and W.L. performed *in vivo* experiment; J.M. H. and S.L. performed transcriptome analysis; S.W.K. conceived the study, interpreted data, and wrote manuscript.

#### Data availability

The RNA sequencing data that support the findings of this study have been deposited in the GEO database (Accession Number: GSE164742). The data that support the findings of this study are available from the corresponding author upon reasonable request. The authors declare that all the data supporting the findings of this study are available within the paper and its supplementary information files.

#### Declaration of competing interest

The authors declare no competing financial interests.

#### Acknowledgements

We thank Drs. Tamas Balla and Bert Vogelstein for live-cell imaging vectors and HCT116 cell lines, respectively. This study was supported by grants from the National Research Foundation of Korea (2018R1A2B3006323 and 2017M3A9B6073098). C.M. was also supported by grants from the National Research Foundation of Korea (2019R111A1A01057557) and the RP-Grant (2018-2019) of Ewha Womans University.

#### Appendix A. Supplementary data

Supplementary data to this article can be found online at <https://doi.org/10.1016/j.redox.2022.102293>.

#### References

- [1] T. Finkel, N.J. Holbrook, Oxidants, oxidative stress and the biology of ageing, *Nature* 408 (2000) 239–247.
- [2] S.D. Dyal, M.T. Brown, P.J. Johnson, Ancient invasions: from endosymbionts to organelles, *Science* 304 (2004) 253–257.
- [3] D.D. Newmeyer, S. Ferguson-Miller, Mitochondria: releasing power for life and unleashing the machineries of death, *Cell* 112 (2003) 481–490.
- [4] D.C. Wallace, Mitochondrial diseases in man and mouse, *Science* 283 (1999) 1482–1488.
- [5] T. Nishikawa, D. Edelstein, X.L. Du, S. Yamagishi, T. Matsumura, Y. Kaneda, M. A. Yorek, D. Beebe, P.J. Oates, H.P. Hammes, I. Giardino, M. Brownlee, Normalizing mitochondrial superoxide production blocks three pathways of hyperglycaemic damage, *Nature* 404 (2000) 787–790.
- [6] M. Schieber, N.S. Chandel, ROS function in redox signaling and oxidative stress, *Curr. Biol.* 24 (2014) R453–R462.
- [7] C. Gargioli, G. Turturici, M.M. Barreca, W. Spinello, C. Fuoco, S. Testa, S. Feo, S. M. Cannata, G. Cossu, G. Sconzo, F. Geraci, Oxidative stress preconditioning of mouse perivascular myogenic progenitors selects a subpopulation of cells with a distinct survival advantage *in vitro* and *in vivo*, *Cell Death Dis.* 9 (2018) 1.
- [8] S. Pasupathy, S. Homer-Vanniasinkam, Ischaemic preconditioning protects against ischaemia/reperfusion injury: emerging concepts, *Eur. J. Vasc. Endovasc. Surg. : the official journal of the European Society for Vascular Surgery* 29 (2005) 106–115.
- [9] K.A. Reimer, C.E. Murry, R.B. Jennings, Cardiac adaptation to ischemia. Ischemic preconditioning increases myocardial tolerance to subsequent ischemic episodes, *Circulation* 82 (1990) 2266–2268.
- [10] B. Bukau, A.L. Horwich, The Hsp70 and HSP60 chaperone machines, *Cell* 92 (1998) 351–366.
- [11] F. Cappello, E.C. de Macario, L. Marasa, G. Zummo, A.J. Macario, HSP60 expression, new locations, functions, and perspectives for cancer diagnosis and therapy, *Cancer Biol. Ther.* 7 (2008).
- [12] D. Chandra, G. Choy, D.G. Tang, Cytosolic accumulation of HSP60 during apoptosis with or without apparent mitochondrial release: evidence that its pro-apoptotic or pro-survival functions involve differential interactions with caspase-3, *J. Biol. Chem.* 282 (2007) 31289–31301.
- [13] S.K. Calderwood, S.S. Mambula, P.J. Gray Jr., Extracellular heat shock proteins in cell signaling and immunity, *Ann. N. Y. Acad. Sci.* 1113 (2007) 28–39.
- [14] J.N. Chun, B. Choi, K.W. Lee, D.J. Lee, D.H. Kang, J.Y. Lee, I.S. Song, H.I. Kim, S. H. Lee, H.S. Kim, N.K. Lee, S.Y. Lee, K.J. Lee, J. Kim, S.W. Kang, Cytosolic HSP60 is involved in the NF- $\kappa$ B-dependent survival of cancer cells via IKK regulation, *PLoS One* 5 (2010), e9422.
- [15] J.L. Luo, H. Kamata, M. Karin, IKK/NF- $\kappa$ B signaling: balancing life and death—a new approach to cancer therapy, *J. Clin. Invest.* 115 (2005) 2625–2632.
- [16] M.S. Hayden, S. Ghosh, Signaling to NF- $\kappa$ B, *Genes Dev* 18 (2004) 2195–2224.
- [17] G.B. Waypa, J.D. Marks, R. Guzy, P.T. Mungai, J. Schriewer, D. Kocik, P. T. Schumacker, Hypoxia triggers subcellular compartmental redox signaling in vascular smooth muscle cells, *Circ. Res.* 106 (2010) 526–535.
- [18] S.E. Schriener, N.J. Linford, G.M. Martin, P. Treuting, C.E. Ogburn, M. Emond, P. E. Coskun, W. Ladiges, N. Wolf, H. Van Remmen, D.C. Wallace, P.S. Rabinovitch, Extension of murine life span by overexpression of catalase targeted to mitochondria, *Science* 308 (2005) 1909–1911.
- [19] P. Varnai, X. Lin, S.B. Lee, G. Tuymetova, T. Bondeva, A. Spat, S.G. Rhee, G. Hajnoczky, T. Balla, Inositol lipid binding and membrane localization of isolated pleckstrin homology (PH) domains. Studies on the PH domains of phospholipase C delta 1 and p130, *J. Biol. Chem.* 277 (2002) 27412–27422.
- [20] S.W. Tait, D.R. Green, Mitochondria and cell death: outer membrane permeabilization and beyond, *Nat. Rev. Mol. Cell Biol.* 11 (2010) 621–632.
- [21] J.Q. Kwong, J.D. Molkenin, Physiological and pathological roles of the mitochondrial permeability transition pore in the heart, *Cell Metabol.* 21 (2015) 206–214.
- [22] T. Kuwana, D.D. Newmeyer, Bcl-2-family proteins and the role of mitochondria in apoptosis, *Curr. Opin. Cell Biol.* 15 (2003) 691–699.
- [23] O. Soderberg, M. Gullberg, M. Jarvius, K. Ridderstrale, K.J. Leuchowius, J. Jarvius, K. Wester, P. Hydbring, F. Bahram, L.G. Larsson, U. Landegren, Direct observation of individual endogenous protein complexes *in situ* by proximity ligation, *Nat. Methods* 3 (2006) 995–1000.
- [24] R. Ishida, T. Okamoto, F. Motojima, H. Kubota, H. Takahashi, M. Tanabe, T. Oka, A. Kitamura, M. Kinjo, M. Yoshida, M. Otaka, E. Grave, H. Itoh, Physicochemical properties of the mammalian molecular chaperone HSP60, *Int. J. Mol. Sci.* 19 (2018).
- [25] J.H. Seo, E. Agarwal, Y.C. Chae, Y.G. Lee, D.S. Garlick, A.M. Storaci, S. Ferrero, G. Gaudioso, U. Gianelli, V. Vaira, D.C. Altieri, Mitochondrial fission factor is a novel Myc-dependent regulator of mitochondrial permeability in cancer, *EBioMedicine* 48 (2019) 353–363.
- [26] H. Zhou, J. Wang, P. Zhu, H. Zhu, S. Toan, S. Hu, J. Ren, Y. Chen, NR4A1 aggravates the cardiac microvascular ischemia reperfusion injury through suppressing FUNDC1-mediated mitophagy and promoting Mff-required mitochondrial fission by CK2 $\alpha$ , *Basic Res. Cardiol.* 113 (2018) 23.
- [27] E.Q. Toyama, S. Herzog, J. Courchet, T.L. Lewis Jr., O.C. Loson, K. Hellberg, N. P. Young, H. Chen, F. Polleux, D.C. Chan, R.J. Shaw, Metabolism. AMP-activated protein kinase mediates mitochondrial fission in response to energy stress, *Science* 351 (2016) 275–281.
- [28] B. Canovas, A.R. Nebreda, Diversity and versatility of p38 kinase signalling in health and disease, *Nat. Rev. Mol. Cell Biol.* 22 (2021) 346–366.
- [29] M.B. Menon, J. Gropengiesser, J. Fischer, L. Novikova, A. Deuretzbacher, J. Lafera, H. Schimmeck, N. Czymmeck, N. Ronkina, A. Kotlyarov, M. Aepfelbacher, M. Gaestel, K. Ruckdeschel, p38(MAPK)/MK2-dependent phosphorylation controls cytotoxic RIPK1 signalling in inflammation and infection, *Nat. Cell Biol.* 19 (2017) 1248–1259.
- [30] M.C. Morris, J. Depollier, J. Mery, F. Heitz, G. Divita, A peptide carrier for the delivery of biologically active proteins into mammalian cells, *Nat. Biotechnol.* 19 (2001) 1173–1176.
- [31] A.A. Beg, Endogenous ligands of Toll-like receptors: implications for regulating inflammatory and immune responses, *Trends Immunol.* 23 (2002) 509–512.
- [32] A.T. Kwon, D.J. Arenillas, R. Worsley Hunt, W.W. Wasserman, oPOSSUM-3: advanced analysis of regulatory motif over-representation across genes or ChIP-Seq datasets, *G3 (Bethesda)* 2 (2012) 987–1002.

- [33] T. Lu, D.I. Gabrilovich, Molecular pathways: tumor-infiltrating myeloid cells and reactive oxygen species in regulation of tumor microenvironment, *Clin. Cancer Res.* 18 (2012) 4877–4882.
- [34] E.C. Cheung, G.M. DeNicola, C. Nixon, K. Blyth, C.F. Labuschagne, D.A. Tuveson, K.H. Vousden, Dynamic ROS control by TIGAR regulates the initiation and progression of pancreatic cancer, *Cancer Cell* 37 (2020) 168–182 e164.
- [35] J.C. Goldstein, N.J. Waterhouse, P. Juin, G.I. Evan, D.R. Green, The coordinate release of cytochrome c during apoptosis is rapid, complete and kinetically invariant, *Nat. Cell Biol.* 2 (2000) 156–162.
- [36] T. Kuwana, M.R. Mackey, G. Perkins, M.H. Ellisman, M. Latterich, R. Schneider, D. R. Green, D.D. Newmeyer, Bid, Bax, and lipids cooperate to form supramolecular openings in the outer mitochondrial membrane, *Cell* 111 (2002) 331–342.
- [37] K. McArthur, L.W. Whitehead, J.M. Heddleston, L. Li, B.S. Padman, V. Oorschot, N. D. Geoghegan, S. Chappaz, S. Davidson, H. San Chin, R.M. Lane, M. Dramicanin, T. L. Saunders, C. Sugiana, R. Lessene, L.D. Osellame, T.L. Chew, G. Dewson, M. Lazarou, G. Ramm, G. Lessene, M.T. Ryan, K.L. Rogers, M.F. van Delft, B.T. Kile, BAK/BAX macropores facilitate mitochondrial herniation and mtDNA efflux during apoptosis, *Science* 359 (2018) 883.
- [38] J. Kim, R. Gupta, L.P. Blanco, S. Yang, A. Shteinifer-Kuzmine, K. Wang, J. Zhu, H. E. Yoon, X. Wang, M. Kerkhofs, H. Kang, A.L. Brown, S.J. Park, X. Xu, E. Zandee van Rilland, M.K. Kim, J.I. Cohen, M.J. Kaplan, V. Shoshan-Barmatz, J.H. Chung, VDAC oligomers form mitochondrial pores to release mtDNA fragments and promote lupus-like disease, *Science* 366 (2019) 1531–1536.
- [39] X. Guo, G. Aviles, Y. Liu, R. Tian, B.A. Unger, Y.T. Lin, A.P. Wiita, K. Xu, M. A. Correia, M. Kampmann, Mitochondrial stress is relayed to the cytosol by an OMA1-DELE1-HRI pathway, *Nature* 579 (2020) 427–432.
- [40] E. Fessler, E.M. Eckl, S. Schmitt, I.A. Mancilla, M.F. Meyer-Bender, M. Hanf, J. Philippou-Massier, S. Krebs, H. Zischka, L.T. Jae, A pathway coordinated by DELE1 relays mitochondrial stress to the cytosol, *Nature* 579 (2020) 433–437.
- [41] R. Liu, D.C. Chan, The mitochondrial fission receptor Mff selectively recruits oligomerized Drp1, *Mol. Biol. Cell* 26 (2015) 4466–4477.
- [42] M. Fiore, S. Forli, F. Manetti, Targeting mitogen-activated protein kinase-activated protein kinase 2 (MAPKAPK2, MK2): medicinal chemistry efforts to lead small molecule inhibitors to clinical trials, *J. Med. Chem.* 59 (2016) 3609–3634.